Wisconsin Initiative on Climate Change Impacts

Climate Working Group Report:

Climate Change in Wisconsin

Climate Working Group:

Christopher Kucharik[1,2], Co-Chair

Daniel J. Vimont[3,4], Co-Chair

Kathleen Holman[3,4]

Ed Hopkins[5]

David Lorenz[4]

Michael Notaro[4]

Steve Vavrus[4]

John Young[3,5]

December, 2010

[1] University of Wisconsin – Madison Agronomy Department

[2] University of Wisconsin Nelson Institute for Environmental Studies
Center for Sustainability and the Global Environment (SAGE)

[3] University of Wisconsin – Madison Atmospheric and Oceanic Sciences Department

[4] University of Wisconsin Nelson Institute for Environmental Studies
Center for Climatic Research (CCR)

[5] Wisconsin State Climatology Office

Table of Contents

1. Introduction

Wisconsin's geographical setting gives rise to a rich set of climatic conditions that help shape our state's environmental, social and economic resources. In the coming decades, we can anticipate that these influences on state resources will be affected in both expected and unexpected ways as our climate changes. Understanding aend assessing these climate changes requires *(i)* expertise in previous climate changes, *(ii)* understanding of global climate projections – including their uncertainty, and *(iii)* understanding how these global projections relate to regional scale variables that are relevant for policy analysts and policy makers. The mission of the Wisconsin Initiative on Climate Change Impact (WICCI) Climate Working Group (CWG) is listed in the CWG Charter:

> *The Climate Working Group will operate within the Wisconsin Initiative on Climate Change Impacts (WICCI) to assess the current and future state of Wisconsin's climate as well as previous climate changes using a blend of station observations, other existing data sources, and Global Circulation Model (GCM) projections from the IPCC. The Climate Working group will also interact with other standing WICCI working group researchers to provide support and guidance on how to properly interpret previous and current climate data, the downscaled and de-biased GCM projections of 21st climate, and other relevant climate information that is provided in pursuit of each working group's scientific goals.*

The CWG was established in 2008, and consists of scientists in the Nelson Institute for Environmental Studies Center for Climatic Research (CCR) and Center for Sustainability and the Global Environment (SAGE), as well as the University of Wisconsin – Madison Agronomy Department, and the Atmospheric and Oceanic Sciences Department. The CWG's website (http://ccr.aos.wisc.edu/cwg) contains additional information and maps related to climate change in Wisconsin. The work undertaken by the CWG also benefitted greatly from interaction with the Wisconsin State Climatology Office (SCO; a good deal of information about Wisconsin's climate, or data describing Wisconsin's climate, can be found through the SCO website at http://www.aos.wisc.edu/~sco). Results presented herein represent work that was completed in fulfillment of grants from the Wisconsin Focus on Energy Environmental and Economic Development Program in 2006 and 2008, as well as a grant from the Center for Disease Control.

This document describes CWG progress in documenting and understanding past climate change, and in developing state-specific projections of climate change in Wisconsin. Section 2 describes historical changes in Wisconsin climate. Future projections of Wisconsin's climate are described, including methodology for developing those projections, in Section 3. Section 4 summarizes results, and is followed by more detailed description of methodologies in a set of Appendices.

2. Historical Changes

a. Overview of approach for spatially interpolated data

(Text is taken directly from Kucharik et al., in press, 2010)

Wisconsin is characterized by generally minor topographic variations, with gently rolling landscapes so that elevation changes do not play a large role in driving the average climate regime across the state. Lake Superior and Michigan, however, can have significant impacts on seasonal (i.e. traditional meteorological three month seasons) temperature and precipitation (Moran and Hopkins, 2002). Time-series of daily weather observations across Wisconsin of maximum temperature, minimum temperature, and total precipitation for the 1950-2006 time period were previously interpolated to a terrestrial 5-min x 5-min grid (0.0833º lat x 0.0833º lon) using an inverse distance-weighting (IDW) algorithm to generate a continuous 57-year time series of gridded daily weather (Serbin and Kucharik, 2009). Station data were obtained from the NOAA cooperative (COOP) observer network, available from the NCDC website (http://www.ncdc.noaa.gov/oa/ncdc.html/). The COOP stations used were distributed relatively evenly with a slightly lower station density towards the northern part of the state. Additional COOP stations from Illinois, Iowa, Michigan and Minnesota that were within 70-km of the Wisconsin state boundary were also used to mitigate edge effects during statistical interpolation. Stations that did not have at least 53 years of data record (during 1950-2006) were removed to avoid synthetic bias through the addition of stations during the time period of interpolation. Approximately 133 temperature and 176 precipitation stations were used in the development of the dataset, giving an average distance between observing stations of 25.0 km for temperature, and 21.2 km for precipitation. We performed a rigorous test of the predictive accuracy of the IDW gridded surfaces using 104 stations withheld in the production of the climate grids in a post-gridding validation step (see Appendix A).

Simple linear regression analysis (using a least-squares approach) was used to calculate time dependent trends of meteorological variables for annual and seasonal (winter – Dec, Jan, Feb; spring – Mar, Apr, May; summer – Jun, Jul, Aug; fall – Sep, Oct, Nov) maximum and minimum temperature, diurnal temperature range, and total precipitation for each grid cell. Simple linear regression was also used to compute changes in (1) the date of last spring and first fall freeze (0ºC threshold) and the growing season length between those dates (days); (2) growing degree days (GDD, base 10ºC); (3) heating and cooling degree days (HDD and CDD, respectively) using a base temperature of 18.33ºC (65ºF); (4) the total number of days each year with minimum temperatures less than -17.78ºC (0.0ºF) and greater than 32.22ºC (90ºF); and (5) an indication of the onset of spring, approximated by a 10-day running mean temperature reaching 10ºC (50ºF). Growing degree day calculations were performed with a base temperature of 10ºC because this is a commonly used index for calculating thermal time for summer row crops grown in the region (e.g., corn), and heating and cooling degree day calculations assuming the base temperature of 65ºF (18.33ºC) correspond to the methodology used by the National Weather Service. The 10-day running mean temperature of 10ºC was chosen as an onset of spring because it is approximately correlated with the calendar date when corn is planted across southern and central Wisconsin, and 10ºC is also corn seed germination temperature.

b. Historical climate change from spatially interpolated data

(Text is taken directly from Kucharik et al., in press, 2010)

Trends in annually averaged precipitation and mean, maximum, and minimum temperatures are shown in Figure 1. Annual average precipitation has increased by approximately 50 to 100 mm (~5-15%) across large portions of Wisconsin (statewide average of 79.0 mm), with the highest increases in the west central and a corridor from south central regions to the northeast. Sections of the northwest and north central were the only regions that saw declines in annual average precipitation of ~25-50 mm, but the trends were not significant. Annual average temperatures increased by 0.3ºC to 1.2ºC ($p < 0.1$) over a large portion of the state in a corridor from the northwest and west central through the east central counties and down the western shore of Lake Michigan in Milwaukee, Waukesha, Racine, and Kenosha counties. In the northeast, annual average temperatures decreased approximately -0.1ºC to -0.3ºC, but were not significant. Annual average maximum temperature has increased by 0.3ºC to 0.9ºC across portions of the northwest, west central and central part of the state, along with a small portion of the lakeshore counties from Manitowoc to Milwaukee. A smaller region in the northwest and central had significant trends ($p < 0.1$) toward warmer daytime highs. Sections of the southwest and northeast saw annual average daytime highs become cooler by -0.3ºC to -0.6ºC, but the trends were significant ($p < 0.1$) only in isolated locations. Overall, the state annual average trend in daily high temperature was 0.21ºC, and the annual average trend in daily low temperature was 1.0ºC.

(i) Seasonal precipitation trends

Wintertime precipitation has increased by 10-20mm across most of Wisconsin from 1950 to 2006 (statewide average of 13.5 mm), but the trends were generally weak with only a few isolated locations being significant ($p < 0.1$). In springtime, precipitation has increased by 20 to 60 mm across the southern and western portions of the state, with a few geographic regions across the north experiencing a trend towards somewhat drier conditions (-10 mm). However, the only significant trends were for increased precipitation in a small part of south central Wisconsin near Sauk and Dane Counties. Overall, the state average springtime precipitation trend was 14.9 mm. Summer precipitation has increased by 30 to 60mm across the large majority of the southern two-thirds of Wisconsin in which the trends within a smaller region running from the southwest to northeast were significant. However, a rather striking contrast was found across the northern one-third of the state, which has seen a trend towards decreasing summer precipitation of 30 to 60mm, with significant trends across the region near the Michigan border. A small portion of the southeast corner of the state has also seen a significant trend towards less summer precipitation. The entire state has experienced a trend towards more precipitation during the autumn of 10 to 80mm, and across approximately the northwest one-half of the state from LaCrosse to Green Bay, these changes have been significant ($p < 0.1$). The state average autumn precipitation trend was 48.1 mm, which was the most significant increase.

(ii) Seasonal maximum temperature trends

Wintertime daily average maximum temperatures have increased by 0.2ºC to 2.0ºC over almost all of Wisconsin (statewide average of 0.97ºC), with the largest magnitude of changes ($p < 0.1$) located in the central and west central regions. There have been no significant trends towards cooler wintertime daytime high temperatures. Springtime daily average maximum temperatures have increased by 0.5ºC to 1.5ºC across most of the state, with the exception being the far northeast counties north of Green Bay (statewide average of 0.77ºC). Significant trends ($p < 0.1$) were found in the central and west central locations. Summer daily average maximum

temperatures have generally decreased by 0.2ºC to 1.0ºC across most of the state, with some exceptions in portions of the northwest and central (statewide average of -0.36ºC). The trend towards cooler summer daytime highs was most significant ($p < 0.1$) in the southwest corner and northeast section of the state where the magnitude was approximately -1.0ºC. Autumn daily average maximum temperatures have decreased by 0.2ºC to 1.4ºC across most of the state. Similar to summer spatial patterns, the trend towards cooler autumn daytime highs was most significant ($p < 0.1$) in the southwest corner and northeast section of the state were the magnitude was approximately -1.0 to -1.4ºC. The overall statewide average trend for autumn daily high temperatures was -0.59ºC.

(iii) Seasonal minimum temperature trends

Wintertime daily average minimum temperatures have increased by 1.0ºC to 3.5ºC over most of Wisconsin, with the largest magnitude of changes ($p < 0.1$) located in the central regions through the entire western portion of the state. There is a general absence of significant trends towards cooler wintertime nighttime low temperatures, and the statewide average seasonal minimum temperature change for winter was highest out of all temperature trends analyzed (1.85ºC). Springtime daily average minimum temperatures have increased by 0.3ºC to 1.5ºC across most of the state (statewide average of 1.13ºC), and significant trends ($p < 0.1$) were found in 64% of all grid cells, mostly concentrated in a large corridor from the western portions of the state, through the central and east central counties. Summer daily average minimum temperatures have increased by 0.5ºC to 1.3ºC across most of the state (statewide average of 0.83ºC), with the most significant trends ($p < 0.1$) in a corridor from the northwest and west central portions of the state, through the east central counties. A few isolated regions saw a trend towards cooler summer temperatures. Autumn daily average minimum temperatures have decreased by 0.5ºC to 0.7ºC across northeast and southern portions of the state, but the corridor from the northwest and west central through the east central part of the state experienced increases of 0.1ºC to 0.5ºC (statewide average of only 0.02ºC). The trend towards cooler autumn nighttime lows was most significant ($p < 0.1$) in small sections of the south central and far northeast near at the Michigan border. Significant increases in nighttime lows during autumn were also noted in the far southeast counties near Milwaukee, Racine, and Kenosha.

(iv) Extreme temperature trends

Spatial maps of the trend in extreme temperatures across Wisconsin are shown in Figure 2. In general, the majority of Wisconsin has seen a significant trend towards a fewer number of days each year with daily minimum temperatures below -17.8ºC (0.0ºF). The rate of annual occurrence of these extremely cold temperatures has declined by a total of 5 days across the south and northeast, and -15 to -20 days in the far northwest corner of the state. These trends are significant ($p < 0.1$) for approximately 54% of the state, predominantly in the northwest, west central and central regions, and the statewide average rate of change was -9.5 days. In general, the annual frequency of daily maximum temperatures greater than 32.2ºC (90ºF) has not changed significantly from 1950 to 2006 across Wisconsin; the statewide average change was only -0.3 days. Across the southwest through northeast part of the state, there has been a small trend towards a fewer number of days each year greater than 32.2ºC, but large portions of the central and northwest have seen a slight increase in the annual occurrence of these very warm daily high

temperatures, but the majority of these changes have been insignificant; only 0.5% of all grid cells had a significant trend.

(v) Last spring freeze, first fall freeze, and growing season

Trends in the date of the last spring freeze, first fall freeze, growing season, and onset of spring are shown in Figure 3. In general, most of the state of Wisconsin has experienced a trend towards an earlier occurrence of the last spring freeze date (0.0ºC, 32ºF threshold) by about 2 to 10 days, with an overall statewide average of -5.6 days. The most significant changes have occurred in the southwest corner, the central through northeast region, as well as the extreme northwest counties. In the far northwest, the date of the last spring freeze has retreated by up to two weeks in just 57 years. Less significant trends were found across most of the southeast portion of the state. The lakeshore region in the Milwaukee and Racine area had a significant trend towards an earlier occurrence of the last spring freeze date by about one week. Most of the central, northeast and northwest part of Wisconsin has experienced a trend towards a later date of occurrence of the first fall freeze (0.0ºC, 32ºF threshold) by about 3 to 12 days. Less significant trends were found across most of the southeast and extreme southwest portion of the state near the Mississippi River. A total of 55% of all grid cells had a significant trend in fall freeze date, with an overall state average of 6.5 days later. Some of these regions actually saw a trend towards an earlier arrival of the first fall freeze date, but those trends were not significant. These spring and fall freeze date trends, which are diverging in many regions of the state, have led to a highly significant increase in the length of the growing season in many locations. The largest trends are located in the northwest and central regions, were typically the growing season has been extended by two to three weeks, with some counties in the extreme northwest seeing the growing season lengthen by about four weeks in 57 years, or about 5 days per decade. The western counties near the Mississippi River, the south central, southeast, and east central counties have experienced insignificant changes in the growing season length. The Milwaukee metropolitan area is the exception in the southeast where it appears the growing season trend is significant, and has lengthened by approximately 10 days from 1950 to 2006. The statewide average change in growing season length was 12.0 days longer, and 59% of all grid cells had a significant trend.

(vi) Onset of spring

In order to better understand whether significant changes in the arrival of spring have occurred, changes in the date when a 10-day running mean daily temperature threshold of 10ºC (50ºF) was reached were studied. This might be a more robust indication of sustained changes in spring onset rather than using a single day threshold like the last spring freeze date. In general, the majority of the state – southwest of a Manitowoc to Ashland line has experienced an earlier onset of spring. The most significant changes have been found in the southern half of the state, where the date of occurrence of spring onset has become earlier by 3 to approximately 10 days. While the northeast and north central portion of the state has seen a minimal trend towards a later onset of spring of about 1 to 4 days over 57 years, those trends were not significant. The statewide average change in spring onset date was -4.1 days.

(vii) Concluding remarks

During the 1950-2006 period across Wisconsin, significant changes in climate have occurred, but the spatial patterns and magnitude of these changes vary significantly from location to location. In general, the most widely applicable statement that can be made about climate change in Wisconsin is that the state's residents are experiencing a trend towards wetter conditions with less extreme cold, but the number of extremely hot days during summer does not appear to have increased. The four seasons have experienced widely varying degrees of climate change, with the most pronounced warming having occurred in winter and spring, and nighttime low temperatures are increasing at a rate that is faster than daytime highs. The difference in the rate of warming between daytime and nighttime temperatures has caused the diurnal temperature range to compress by 0.35ºC in springtime to as much as 1.2ºC in summertime. The growing season has become longer by about 1 to 3 weeks across the interior portion of the central and northern parts of the state. The Tension Zone appears to have shifted slightly to the north and northeast by a modest 15 to 20 km, but suggests that continued climate change could pose a threat to the distribution of vegetation and animal species in the region, as well as have an impact on productivity of our croplands and forests. The increase in CDDs and decrease in HDDs have likely impacted energy usage and heating and cooling demands, but might be overshadowed by increasing consumption by residents of the state for everyday energy use.

In future studies, an extension of the current study to a larger region in the Midwest is anticipated to better understand whether the patterns observed across Wisconsin are connected to larger patterns or drivers in the Great Lakes region. The results presented here are meant to provide policy makers, land managers, and scientists a starting point to discuss recent climate change across Wisconsin, and how these changes, if they were to continue, might impact the broader natural resources, industry, and future planning in the state of Wisconsin. Furthermore, the results are also intended to help climate scientists better understand the robustness of GCM output for the region, and provide the initial basis for discussions about where discontinuities exist between the recent historical record of change and what is projected to occur in the future.

c. Observed changes in heavy precipitation events

An important but unresolved question is how extreme weather differs as climate changes. This issue is particularly a concern for heavy precipitation events, whose frequency and magnitude are expected to increase in a warming climate, due to the rise in atmospheric moisture content (Trenberth 1999). The recent assessment report on weather extremes issued by the U.S. Climate Change Science Program states, "One of the clearest trends in the U.S. observational record is an increasing frequency and intensity of heavy precipitation events" (Karl et al. 2008). This nationwide change during the past decades to century includes Wisconsin (Groisman et al. 2004, 2005; Madsen 2007). Madison in particular has experienced a large number of heavy precipitation events in the past decade: 24 days of 2" or more rainfall (compared with the previous decadal maximum of 12 since the 1950s) and 8 days of 3" or more rainfall (nearly as many days as the five previous decades combined). This result is consistent with the 50% rise in frequency of 4-inch daily rainfalls in the upper Midwest over the last century reported by Groisman et al. (2001).

The frequency of daily precipitation amounts exceeding 1", 2", and 3" from 1950-2008 at six major airport weather stations in the central and southern portions of the state – Eau Claire, Green Bay, La Crosse, Madison, Milwaukee, and Wausau – shows a positive trend in 16 of the 18 time series (Figure 4). These increases in intense events generally agree with the wetter mean conditions with time, although only two of the records show a statistically significant increase in heavy precipitation based on the stringent Mann-Kendall trend detection test (1" events at Milwaukee and La Crosse). There is a strong correlation between mean decadal precipitation and the decadal frequency of 1" events (six-station average of $r = 0.84$), whereas the less common 2" and 3" events are less highly correlated with the mean ($r = 0.39$ and 0.33, respectively), suggesting that they are more stochastic occurrences (Kucharik et al., 2010).

Trends in extreme temperatures have differed strongly with regard to severe heat vs. cold during the past half century, as described in detail by Kucharik et al. (2010). The occurrence of daily minimum temperatures below 0°F has declined sharply in most of Wisconsin, with nearly all locations showing downward trends between 1950 and 2006 (Figure 5). The decline has been most pronounced in the northwest, where a 15 to 20 day decrease has occurred, but most of Wisconsin (54%) has experienced a statistically significant negative trend in the frequency of extremely cold nights (statewide average = -9.5 days). Conversely, hot days (daily maximum above 90°F) have not shown a clear trend during the same time period (Figure 5). The statewide mean downward trend of 0.3 days is a near balance between small increases of 2 to 3 days primarily in the northwest and modest decreases of 3 to 4 days mostly over the extreme southwest and Fox Valley. Statistically significant trends in hot days have occurred across less than 1% of Wisconsin.

Compared with national and global trends, these regional changes in extremes are similar for precipitation but different with respect to temperature. As discussed in Alexander et al. (2006), most regions of the world have experienced more heavy rainfall and hot days but less bitter cold in recent decades (1951-2003). Eastern North America, however, stands out as an anomalous pocket that has no significant areally averaged trends in extreme temperature. The central U.S., including half of Wisconsin, even had no mean warming during the past century, a phenomenon referred to as the "warming hole" (Kunkel et al. 2006). By contrast, heavy precipitation has increased over almost the entire eastern half of the U.S. (Alexander et al. 2006).

Although evidence is robust that heavy precipitation has generally been increasing, the starting point of most studies is typically the middle 20th century (Alexander et al. 2006; Kucharik et al. 2010) or the very late 1800s (Groisman et al. 2001; Kunkel et al. 1999, 2003). This time constraint limits our ability to place into proper historical perspective the recent observed increases in heavy precipitation and thus complicates efforts to attribute unequivocally greenhouse warming as a cause of the secular trend. Indeed, there is evidence of low-frequency variability on approximately century time scales, based on time series of measured and inferred intense precipitation since the late 1800s (Kunkel et al. 2003; Ken Potter, personal communication) that show relatively wet conditions in the early part of the record, drier in the middle 20th century, and wetter since. Madison's long-term precipitation record displays an upward spike during the 1880s, in agreement with tree-ring and Mississippi River streamflow data, indicating wetter conditions than in any other pentad. Such data warrant caution in attributing recent positive trends in mean and extreme precipitation solely to greenhouse

warming. If adequate records exist, one possible way to assess the relatively wet period in the late 19th century is to determine the extent of the anomalies. High spatial variability would suggest that unusual atmospheric circulation patterns were the primary driver, whereas ubiquitous increases in heavy rainfall are a greenhouse warming signal in climate models, which simulate more intense precipitation over almost all land regions (Meehl et al. 2007). Stations with long-term weather records in and around Wisconsin from the late 19th century---Milwaukee, La Crosse, Chicago, Minneapolis, and St. Louis---do not show the extreme spike in annual precipitation during the 1880s exhibited in the Madison data. Kunkel et al. (2003) found that the relatively high values of intense precipitation nationally averaged during the early part of his record (1895-1905) consisted of high spatial variability, with very large positive anomalies in the western half of the country compared with near-normal conditions in the east, whereas the wet 1990s decade showed a much more uniform pattern of anomalous precipitation throughout the U.S. Similarly, heavy precipitation events have increased during the past five decades over all regions of the country, including Hawaii and Alaska (Karl et al. 2009). Due to the prevalence of natural climatic variability on decadal and centennial time scales and the difficulty in ascribing statistical significance to trends in rare events, further investigation will be necessary before a definitive statement can be made as to the cause(s) of the increase in mean and extreme precipitation over Wisconsin during the past several decades.

3. Projected Climate Change in Wisconsin

In this section we describe projected changes in Wisconsin's climate by mid and late 21st century. We present results that have been statistically downscaled from the global climate models that contribute daily output to the World Climate Research Programme's (WCRP's) Coupled Model Intercomparison Project phase 3 (CMIP3) multi-model dataset (Meehl et al., 2007; these models are the same models that contributed to the IPCC 4th Assessment Report)[1]. Methodology for the downscaling is described in Section 3.a, estimates of uncertainty are described in Section 3.b, future projections of average conditions are described in Section 3.c, and future projections of extreme events are described in Section 3.d.

a. Methodology

(i) Downscaling methodology

The statistical downscaling consists of two stages. First, the statistical relationship between the large-scale atmospheric state and local temperature / precipitation at weather stations is determined for each calendar month from the observational record (1950-2007). Second, this established statistical relationship is applied to predict the local temperature / precipitation given a climate model's large-scale atmospheric state. The relationship between the large-scale atmospheric state and the weather stations is cross validated for all variables and seasons by

[1] We acknowledge the modeling groups, the Program for Climate Model Diagnosis and Intercomparison (PCMDI) and the WCRP's Working Group on Coupled Modelling (WGCM) for their roles in making available the WCRP CMIP3 multi-model dataset. Support of this dataset is provided by the Office of Science, U.S. Department of Energy.

alternately leaving out three years of data, fitting the remaining years and testing the fit on the left out data. The cross validation suggests that all statistical relationships found are robust.

Typically, statistical downscaling is used to relate the large-scale atmospheric state to one specific value of the temperature / precipitation at a point. With this approach, however, the downscaled variability and extremes at the point will be too small unless the relationship between the large-scale and the point is artificially inflated (von Storch 1999), which then artificially exaggerates the climate change resulting from changes in the large-scale. Therefore, in order to both simulate the variability and extremes *and* to properly account for the effect of the large-scale on the weather at a point, we relate the large-scale atmospheric state to the Probability Density Function (PDF) of temperature / precipitation at a point instead of a single value of temperature / precipitation. This approach takes into account that the large-scale atmospheric state does not completely specify the evolution of the atmosphere at small scales, instead the large-scale specifies the range and likelihood of particular outcomes at a point. To create a specific downscaled time series of temperature / precipitation at a point, we draw random numbers from the particular PDF for each individual day in the record. Obviously, there are an infinite number of possible time series given the large-scale atmospheric evolution. We call these possible outcomes *realizations*.

For maximum and minimum temperature, we use linear regression to relate large-scale maximum / minimum temperature to local maximum / minimum temperature. In classical linear regression, the errors in the linear 'fit' between the predictand and the predictor are assumed to be a Gaussian distribution with variance equal to the error variance. This Gaussian distribution with mean given by the linear 'fit' and constant error variance is the PDF of local temperature given the large-scale. Note that linear regression only assumes that the *errors* from the linear fit are Gaussian. Although the temperature in certain seasons can be strongly skewed, we find that the large-scale temperature is also strongly skewed so that linear regression actually works quite well.

For precipitation, we use two separate statistical models: one for the occurrence of precipitation (is the day wet or dry?) and the other for the amount of precipitation if the day is wet. Because the distributions of both precipitation occurrence and precipitation amount are highly non-normal, we use more flexible statistical models including Generalized Linear Models (GLM) (Nelder and Wedderburn, 1972). For precipitation occurrence, we use the GLM also known as logistic regression. For precipitation amount we find that GLMs are not general enough so we fit the precipitation amount to the generalized gamma distribution (Stacy, 1962) with the scale parameter and one of the shape parameters dependent on the large-scale atmospheric state. Both of these precipitation models are fit using maximum likelihood.

We use the NCEP Reanalysis (Kalnay et al., 1996) for the large scale and the National Weather Service's Cooperative Observer Program's (COOP) for the point observations. The COOP stations within 42.1-47.1°N, 93.4-86.6°W that report at least 83.3% of months during January 1950 to December 2007, and do not exhibit blatant observer biases in precipitation occurrence / weak precipitation (Daly et al., 2007), are included, consisting of a well-distributed network of 170 stations for daily maximum and minimum temperature and 164 stations for daily precipitation. Before applying the fitted relationship between the Reanalysis and the COOP

stations to the climate models, we quantile adjust the climate models' PDFs of the large-scale predictors to remove climate model biases (e.g. Wood et al., 2004).

For this project we have generated three realizations of gridded daily precipitation and maximum and minimum temperature. Instead of interpolating the raw atmospheric variables from the stations to the grid, the parameters of the PDFs are first interpolated to a 0.1 ° x 0.1° grid and then random realizations are generated using the gridded PDFs. This basically eliminates the reduction in variance and extremes that typically occurs when one interpolates the raw data.

(ii) Methodology for calculating results

Results for expected climate change in Wisconsin are constructed from available daily output from the CMIP3 archive. Changes are expressed as the expected average climate change by mid 21st century (2046-2065) and by late 21st century (2081-2100) relative to average conditions over the late 20th century (1961-2000). Results in this analysis are presented for three different future scenarios for greenhouse gas emissions from the Special Report on Emissions Scenarios (SRES; see Nakicenovic et al. 2000): the B2 scenario (low emissions), the A1 scenario (high emissions) and the A1B scenario (moderate to high emissions). Although observed emissions since 1990 have exceeded even the highest of these three scenarios (Raupach et al. 2007), these three scenarios still represent reasonable guesses for expected climate change over the 21st century in the absence of aggressive global mitigation.

The range of climate change for a particular time period and a particular emission scenario is estimated by fitting a probability distribution across all model estimates of a particular change. The range of anticipated climate change is stated as the 10th to 90th percentile (i.e. according to the downscaled model data, there is a 90% chance the change will exceed the 10th percentile, and a 90% chance it will be less than the 90th percentile). The probability distribution is generated by fitting a Gaussian kernel density estimator to the spread of model estimates of climate change. When maps are presented, they usually represent the average climate change across all models.

b. Future climate change in Wisconsin: first order variables

In this section we discuss projected changes in variables that are directly calculated by the downscaling methodology. In Section *(i)* we discuss change in annual and seasonal average precipitation and maximum and minimum temperature. In Section *(ii)* we discuss changes in extreme temperature, and projected changes in extreme precipitation are discussed in Section *(iii)*. Note that further maps and analysis may be found online at: http://ccr.aos.wisc.edu/cwg/ .

(i) Annual and seasonal averages: temperature and precipitation

The projected warming of Wisconsin's climate by mid-21st century under the A1B scenario is depicted in Figure 6. Mean temperature (estimated as an average of daily high and nighttime low temperatures) is expected to warm across the state by about 3.5 °C (6.3 °F), with minimally more warming in the central and western parts of the state. The estimate of 3.5 °C represents the average warming across all models. But, there is a range of possible warming as simulated by different models. The cumulative distribution across model simulations of annual mean

warming is depicted in Fig. 7, and shows that Wisconsin's climate is projected to warm between 2 °C (4 °F) and 5 °C (9 °F). This range represents the 10th to 90th percentiles of model warming, and is often more appropriate for planning purposes than the mean warming described above.

The expected mean temperature change for mid 21st century conditions does not depend too sensitively on the emissions scenario, although we generally do not advise direct comparisons between the A2 scenario and the other two scenarios as different models contribute to the A2 scenario. The projected change in mean temperature for the A2 scenario is 2°C – 4.5°C, and the projected change for the B1 scenario is 1.25°C - 4°C. By the late 21st century the warming is considerably amplified. Mean warming is projected at 3.5°C – 7.5°C for the A1B scenario, 4°C – 8°C for the A2 scenario, and 2°C – 5.5°C for the B1 scenario.

The downscaled data indicate that, like observed trends, nighttime low temperatures are expected to warm slightly more than daytime high temperatures by mid-21st century. For the A1B scenario under mid 21st century conditions, nighttime low temperatures are expected to increase by about 2.5 – 5.5 °C, and daytime highs should increase by about 2 – 5 °C. Daily mean temperature is inferred by averaging these two numbers together, resulting in the (rounded) mean temperature change reported earlier. These numbers are consistent with raw IPCC projections for the region as well. Changes in daily high and low temperatures are also amplified by the end of the century for the A1B scenario, with changes in daytime highs projected to increase by 3°C - 8°C and nighttime lows projected to increase by 3.5°C – 7.5°C.

Seasonal temperature changes are depicted in Figure 8 and show that the temperature changes are seasonally dependent. For brevity, we report only the results from the A1B scenario here. Winter (Dec – Feb averaged) daytime high temperatures are projected to increase by 2.25 – 5.75 °C, and daytime low temperatures by 3 – 7 °C. During summer (Jun – Aug averaged), daytime high temperatures are projected to increase by 1.25 – 4.25 °C, and nighttime low temperatures by 2 – 5 °C. So, winter temperatures tend to warm more than summer temperatures, and nighttime low temperatures during winter and summer tend to warm more than daytime high temperatures. This is consistent with the observed trends in Wisconsin. During spring (Mar – May), daytime high temperatures are projected to increase by 1.75 – 5.25 °C, and nighttime low temperatures by 1.75 – 5 °C. In Fall (Sep – Nov), daytime high temperatures are projected to increase by 2 – 6 °C, and nighttime low temperatures by 2 – 5 °C. Note that during the "transition" seasons (spring and fall) the daytime high temperatures are projected to increase slightly more than the nighttime lows. The raw output from the global climate models used to downscale precipitation show similar ranges of warming, though they show that the increase in nighttime low temperature exceeds the increase in daytime high temperatures only during winter.

The sign of projected annually averaged precipitation changes is less certain than the sign of temperature changes. The downscaled data suggest that Wisconsin's annually averaged precipitation will change by between -5% and +15%. Note that "no change" in annually averaged precipitation is consistent with the model projections, but that the probability distribution indicates there is a 75% chance that precipitation will increase. When broken down by season (Figure 9), there is considerable agreement that precipitation will increase during winter (0-40% increase), and virtually no agreement during summer (50-50 % chance for an

increase or decrease). Still, the lack of agreement during summer does not imply that there is no information from the models. The models do suggest a change between -20% and +15%. As most of Wisconsin's precipitation comes during the winter season, the summer season changes (and uncertainty) dominates the annually averaged change (and uncertainty). During spring, the projected change is between -5% and +25%, while during fall the projected change is between -5% and +15%. The projected annually averaged precipitation change by late century for the A1B scenario is between -5% and +25%, with winter changes projected between 0% and +40%, and summer precipitation changes projected between -25% and +20%.

(ii) Projected changes in extreme temperatures

Simulations from global climate models indicate that most regions, including Wisconsin, should expect a future with much less extreme cold but considerably more heat waves and heavy precipitation (Meehl et al., 2007). Our downscaled GCM output bears this out and puts these changes into a sharper spatial focus. The projected decline of extreme cold-air outbreaks over the Great Lakes area (Vavrus et al. 2006) and the reduction in snow cover (Notaro et al. 2010) should lead to significantly fewer severely cold days in Wisconsin. Our downscaled model results show decreases in the number of nights below 0ºF throughout the state, even by the middle 21st century. The smallest changes occur in the southeast portion of Wisconsin in all three emissions scenarios and suggest a moderating influence from Lake Michigan in the modern climate (Figure 3). Maximum decreases are simulated across far northern Wisconsin, where sub-zero nights are common during winter in the present climate. The magnitude of the decline in 0ºF nights around the state by the middle of this century ranges from 6 to 18 in the B1 scenario to 9 to 24 (A1B). By the end of the 21st century these frequencies become 9 to 33 nights (A2 scenario) but maintain a similar spatial pattern.

As expected, heat waves in Wisconsin are projected to become more common and severe in the future. The simulated change in the frequency of 90ºF days displays a meridional gradient, with larger increases in the south (Figure 10). The downscaling procedure captures the moderating influence of Lakes Michigan and Superior on extreme heat, leading to locally smaller increases in heat frequency. This tempering effect is especially apparent along the Door Peninsula, where the occurrence of 90ºF days is expected to rise only 4-8 days by mid century and 8-20 days by late century among the three emissions scenarios. Conversely, the maximum increase in hot weather is projected over extreme southern Wisconsin, where models suggest increases of 20-28 days by mid century and 28-56 days by late century. A similar spatial pattern is seen for 100ºF days, but the magnitude of change is muted: gains of 1 day/decade or less in the north and up to 4 days/decade far south by mid century, increasing to 2 days/decade or less and up to 14 days/decade by the end of this century.

The projected statewide-average changes in extreme heat and cold are shown in Figure 11 for all 3 emissions scenarios and both time periods. The increase in hot days (90ºF) exceeds the decrease in cold nights (0ºF), especially by the late 21st century when such bitter cold nearly disappears in the A1B and A2 scenarios (approximately an 80% decrease from the late 20th century). The greater number of hot days is strongly dependent on the emissions scenario by 2081-2100, ranging from an increase of 3 weeks (B1) to 6 weeks (A2) compared with the 20th century mean of 1 week. Very hot days (100ºF or higher) seldom occur in the modern climate

(return period of 7 years) but they are simulated to happen at least once per year in all scenarios in both future time periods and up to 10 days annually in A2 by the end of the century. These projected changes in extreme temperatures are remarkably robust; all the climate models simulate an increase (decrease) in the hot-very hot (cold) days (nights) compared with the late 20th century baseline period.

(iii) Projected Changes in Heavy Precipitation

All of Wisconsin should receive more heavy precipitation in the future. The downscaled model projections suggest that the largest increases will occur in eastern and northern regions and may be enhanced by lake-effect processes (Figure 12). The frequency of 1-inch daily events is expected to increase by as little as 5 days/decade in southwest Wisconsin to a maximum of 10 days/decade (A1B) in the extreme northeast by mid century and from 6 days/decade across western Wisconsin to as much as 14 days/decade over the far north and northeast by the end of this century. The spatial variation in the projected change of 1-inch days is similar to that of mean precipitation (spatial correlation coefficient of 0.80), consistent with the findings of Kucharik et al. (2010) for the observed trends at six stations across the state. Daily rainfall of at least 2 inches should also become more common throughout Wisconsin in a pattern somewhat similar to that for 1-inch events. Decadal frequencies increase by mid-century from an emissions scenario-dependent minimum of 1.6-2.0 days (south and west) to as much as 2.8-3.2 days (far north and east), then rise by late century in approximately the same regions from a low of 2.0-3.6 days to a high of 3.6-5.2 days. The heaviest daily rainfalls (at least 3 inches) are also simulated to increase everywhere in Wisconsin, but the models suggest a much less coherent pattern of change across the state. These rare events are projected to increase by mid century from 0.6-1.05 days/decade in all three emissions scenarios. By late century these values increase further---from 0.75-1.05 days/decade (B1), 1.05-1.50 days/decade (A1B), and 1.05-1.80 days/decade (A2)---indicating a sensitivity of intense precipitation to the magnitude of greenhouse forcing. There is much less agreement between the pattern of change in 3-inch rainfalls and the mean change in precipitation across the state (pattern correlation of only 0.23), similar to the observed relationship in recent decades (Kucharik et al. 2010). If we assume that the pattern of mean precipitation change in Wisconsin can be understood as a function of identifiable meteorological processes (e.g., atmospheric circulation, moisture content, and lake influence), then this weak spatial relationship between changes in mean and extreme precipitation suggests low predictability in the location of future heavy precipitation events, even though model evidence strongly suggests more intense rainfall overall across the state.

The impact of heavy precipitation depends in large part on when it occurs; therefore, the seasonal timing of the changes in these events is important. As with mean precipitation, the climate models indicate that the largest increases in heavy precipitation should occur from autumn through spring. The absence of a projected rise in extremes during peak summer is consistent with the uncertainty surrounding average rainfall expected during that season (section 3.c.*(i)*). By contrast, the other three seasons are to become wetter on average, and this change should be accompanied by more heavy precipitation. For example, the largest increases in the occurrence of 3-inch daily rainfalls in Madison in absolute terms are projected during June, September, and October, while the largest percentage changes (more than a doubling) are expected from November to April (Schuster and Potter, 2010). The primary mechanisms causing the change in

heavy precipitation appear to be significant increases in ambient specific humidity and moisture flux convergence (Holman, 2010).

Although projected increases in heavy precipitation events have been commonly reported in the literature, rarely have distinctions been made between their expected change in frequency relative to intensity. Distinguishing between these two components is worthwhile, however, because impacts may be more sensitive to one type of change than the other. The model output shows that much larger increases in the *frequency* than the intensity of heavy precipitation are likely across Wisconsin, and the models are almost unanimous in the positive sign of both of these changes (Figure 13). The frequency change is sensitive to the climate change signal---increasing more with time and with greenhouse forcing---as well as to the magnitude of the event, such that greater increases are expected for heavier rainfalls. The rate of occurrence of heavy daily precipitation averaged over Wisconsin should rise by over 10% (1-inch events) to nearly 40% (3-inch events) by the middle 21st century and by approximately 10-20% (1-inch events) to in excess of 50% (3-inch events) toward the end of the century. By contrast, the projected increases in the intensity (magnitude) of heavy precipitation, expressed here as the daily precipitation amount corresponding to the annual maximum, are much more modest (Figure 13). These statewide changes in intensity correspond to daily precipitation events of at least 2" and are all less than 10% by mid-century and around 10% by late-century, similar to the results for Madison reported by Schuster and Potter (2010).

c. Future climate changes: second order variables

In this section we discuss projected changes in "second-order" variables. By "second-order", we refer to variables that are calculated from the first-order variables (i.e. from downscaled precipitation, and maximum and minimum temperature). We focus on future projections of *(i)* snow, *(ii)* potential evapotranspiration, and *(iii)* changes in hardiness zones. Snow is calculated by using the first-order variables as inputs to SNOW-17, and potential evapotranspiration is calculated using the Priestley-Taylor (1972) method. Note that changes in hardiness zones are directly related to changes in minimum temperature, and as such are not as dependent on a secondary method of calculation.

(i) Snow projections

The WICCI downscaled temperature and precipitation data, for the late 20th century (20C3M) and both mid- and late 21st century (A2, A1B, and B1 emission scenarios), is used to force the National Weather Service conceptual snow accumulation and ablation model, SNOW-17 (Anderson, 1973, 2002, 2006). For each of 11-15 global climate models and all emission scenarios, three realizations of climate data are used to drive the snow model. Based on these SNOW-17 simulations (Notaro *et al*., 2010b), projected changes in Wisconsin-averaged snowfall, snow depth, and snow cover fraction are shown in Figure 14.

A comparison of the A2, A1B, and B1 snow simulations with those from 20C3M shows reductions in Wisconsin snowfall of 34.0 cm (13.4 inches), 36.1 cm (14.2 inches), and 25.4 cm (10.0 inches), respectively, by the mid-21st century and 57.9 cm (22.8 inches), 53.6 cm (21.1 inches), and 37.4 cm (14.7 inches), respectively, by the late 21st century. The greatest snowfall reductions are projected at the flanks of the snowfall season in November and March-April,

representing a shortening of the season; likewise, the largest projected decreases in Wisconsin snow depth and cover occur in February-March.

According to the SNOW-17 simulations for 20C3M, Wisconsin, on average, maintains a snow pack of at least one inch (2.54 cm) for 140 days, from mid-November to mid-April, peaking in mid-February around 19 cm (Figure 14b). The average duration of a snow pack of at least one inch is projected to reduce by 16, 24, or 28 days by the mid-21st century according to scenarios B1, A1B, and A2, respectively, and by 28, 44, and 50 days by the late 21st century for these scenarios. In most cases, the snow season shortens more in the spring than in the autumn. Similarly, according to the SNOW-17 simulations for 20C3M, Wisconsin maintains a snow cover of at least 50% from late November to late March, representing 119 days (Figure 14c). The average duration of a snow cover of at least 50% is projected to diminish by 22, 38, or 34 days by the mid-21st century according to scenarios B1, A1B, and A2 and by 37, 58, and 68 days by the late 21st century for these scenarios. Based on the A2 scenario, by the late 21st century, an average Wisconsin snow cover of at least 50% might be limited to late December through mid-February, totaling only 50 days.

Projected changes in Wisconsin-averaged snowfall by the end of the 21st century, based on SNOW-17 simulations for the A2 scenario, range from -30.5 cm for the Commonwealth Scientific and Industrial Research Organization Mark version 3.5 (CSIRO-Mk3.5) to -86.4 cm for MIROC-3.2-medres (Figure 15).

Of the 11 GCMs, MIROC-3.2-medres features the largest projected annual warming, +8.7°C, and largest projected decrease in annual precipitation, -11.7 cm, both favoring a reduction in annual Wisconsin snowfall by the end of the century. Alternatively, a more modest snowfall reduction of -30.5 cm is projected for Wisconsin according to SNOW-17 simulations for CSIRO-Mk3.5, given the weakest warming, +4.3°C, and a projected increase in annual precipitation by +9.4 cm. Nonetheless, all SNOW-17 simulations forced by downscaled IPCC model output indicate a projected reduction in Wisconsin snowfall. The correlation between projected changes in annual temperature and annual snowfall for the 11 models under the A2 scenario is -0.93 (Figure 15a), which distinctly relates larger warming with larger snowfall reductions. Likewise, the correlation between projected changes in annual precipitation and annual snowfall is +0.62 (Figure 15b), suggesting that projected increases in precipitation will favor smaller snowfall reductions.

Probability density functions (PDFs) of projected changes in Wisconsin-average annual snowfall are shown in Figure 16 for the A2 and B1 scenarios, by the mid- and late 21st century. For example, based on the A2 emission scenario, by the end of this century, annual snowfall may decrease by 35 to 83 cm (using the 10th and 90th percentiles).

By the mid-21st century, Wisconsin's mean snowfall is projected to decrease by 25.4 cm (-21%) or 34.0 cm (-29%), based on SNOW-17 simulations for scenarios B1 and A2, respectively. By the late 21st century, snowfall is simulated to decrease by 37.3 cm (-31%) or 57.9 cm (-49%) for these scenarios. The snowfall projections substantially diverge between the two scenarios by the end of the century. In general, the absolute reduction in snowfall is greatest across northern

Wisconsin, while the percent reduction is largest across southern Wisconsin where annual mean snowfall is lowest (Figure 17).

The largest reduction in snow depth is projected for March, representing a shortening of the snow season. By the mid-21st century, the mean snow depth in mid-March is projected to decrease by either 6.9 cm (-48%) or 9.4 cm (-68%), for scenarios B1 and A2, respectively (Figure 18). By the late 21st century, the projected reduction in snow depth for these scenarios is 10.2 cm (-68%) or 12.4 cm (-85%). Similar to changes in snowfall in Figure 17, the simulated reduction in mean snow depth for mid-March is greatest in northern Wisconsin, while the percent reduction is larger in southern Wisconsin. The projected percent reduction in snow depth, throughout the entire winter season, is substantially greater than the percent reduction in snowfall, given that the reduction in snow depth reflects both diminished snowfall and accelerated snowmelt.

(ii) Potential evapotranspiration projections

Potential evapotranspiration represents the amount of water that could be evaporated from land, water, and plant surfaces if soil water was unlimited, or the maximum water loss to the atmosphere. It is largely driven by temperature and solar radiation. Results presented here use the widely-accepted Priestley-Taylor (1972) method to estimate daily potential evapotranspiration using the WICCI downscaled climate data. Based on this method, an increase in temperature results in an increase in evapotranspiration, while an increase in atmospheric moisture or cloud cover (evident by a lower diurnal temperature range) results in reduced solar input to the Earth's surface and thus reduced evapotranspiration. Using the downscaled temperature data for Wisconsin, daily potential evapotranspiration is estimated for the late 20th century (20C3M) and mid- and late 21st century (A2, A1B, and B1 emission scenarios) for three realizations of 11-15 global climate models. Given that only maximum temperature, minimum temperature, and precipitation are available in the WICCI downscaled dataset, several approximations are applied in computing potential evapotranspiration, such as relating the difference between the daily maximum and minimum temperature to the amount of solar radiation attenuated by atmospheric moisture and clouds.

Annual-mean potential evapotranspiration is projected to increase across Wisconsin, most notably in spring and then in autumn (Figure 19). This increase in potential evapotranspiration is in response to a projected increase in temperature and solar radiation reaching the surface; the latter is evident by an increase in the springtime and autumnal diurnal temperature range, suggesting less attenuation of incoming radiation by clouds or moisture. During winter and summer, a reduction in the diurnal temperature range indicates a moister atmosphere with more attenuation and less shortwave radiation reaching the surface; this counters the effect of rising temperatures, resulting in small changes in potential evapotranspiration during those seasons.

(iii) Projected changes in Wisconsin's plant hardiness zones and gardening

Projected shifts in the plant hardiness zones and the impact on gardening of perennial plants in Wisconsin are explored in Notaro *et al*. (2010a), and shown in Figure 20. Based on downscaled average annual minimum temperature from the WICCI downscaled climate data, maps of the USDA plant hardiness zones for Wisconsin are produced for the recent historical period (1980-

1999), mid-21st century (2046-2065), and late 21st century (2081-2100) using both A2 and B1 emission scenarios. Presently, zones 3b-5b are found in Wisconsin, with Washburn County as a location representative of zone 3b and Milwaukee County representative of zone 5b.

By the middle of this century, independent of emission scenario, warming will likely shift Wisconsin by one or two zones from the south, with Washburn County becoming zone 4b and Milwaukee County becoming zone 6a. Higher temperatures would make northern Wisconsin more conducive to perennial plants such as common foxglove, garden phlox, yellow archangel, and common periwinkle, which previously flourished further south. Likewise, the transition of southeast Wisconsin into zone 6a by the middle of this century would encourage the more successful incorporation of perennial plants such as climbing aster, stinking gladwin, swamp sunflower, and fringed campion into gardens.

Climate projections between the two emission scenarios diverge by the end of the century, with shifts of two hardiness zones projected for Wisconsin under the more favorable, lower emission scenario versus shifts of three to four zones under the high emission scenario. Based on the low emission scenario, zones 4b-6b would extend across Wisconsin by the end of the century. A more dramatic picture is painted under the high emission scenario by the end of the century, with zones 5b-7a, presently found from central Illinois through northern Mississippi, advancing northward across Wisconsin. Given those conditions, northern Wisconsin gardens may flourish with a dramatically richer variety of perennial flowering plants than presently possible, given the much reduced winter chill, including chrysanthemums, spring starflowers Aaron's beard, and Stoke's aster. Concurrently, perennials normally flourishing in, and representative of, the southern states, including southern maidenhair, Texas sage, confederate roses, and atamasco lilies, may become regular elements of Milwaukee County gardens.

Appendix A: Detailed methodology of creating the dataset (directly from Serbin and Kucharik, 2009)

Time-series of daily climate station observations of maximum temperature (T_{max}), minimum temperature (T_{min}) and total precipitation (P_{Total}) from the cooperative observer (COOP) network for the years 1950-2006 were obtained directly from the National Climatic Data Center (NCDC) website (http://www.ncdc.noaa.gov/oa/ncdc.html/). The longest running stations go back to 1895 although many do not have continuously observed data. The COOP stations used were distributed relatively evenly across Wisconsin with a slightly lower station density towards the north. Stations that did not have at least 53 years of data record (1950-2006) were removed to avoid synthetic bias in long term trend analysis through the addition of stations during interpolation. The retained Wisconsin stations amounted to approximately 46% (144/315) of the potential station data. The remaining independent station observations or validation stations failing to satisfy the long-term temporal restriction were later used to generate a validation data set to examine the predictive accuracy of climate surfaces (See validation section). Some stations in the COOP network only provided precipitation and thus there were more daily precipitation observations then temperature in each climate division. The final data record was comprised of a maximum of 133 T_{max} and T_{min} stations and 176 P_{Total} COOP observation stations within Wisconsin and neighboring states. The number of station-days per climate element also varied slightly between the variables. Station elevation ranged from approximately 179 to 541m. The average first-order (i.e. first nearest neighbor) distance between all primary observation stations was 21.2 km (from 3.2 to 65.4 km) and 25.0 km (from 4.3 to 65.4 km) for precipitation and temperature stations, respectively.

Preprocessing and quality control

Several data quality and consistency checks were performed on the primary station list (i.e. those with ≥ 53 years of generally contiguous data) prior to further data processing steps. The primary station list was filtered separately for temperature and precipitation observations. First, the raw daily T_{max}, T_{min}, and P_{Total} were extracted from the primary station observation data set and checked for quality. Values of precipitation less than zero or flagged as erroneous values were replaced with a missing data flag value. In addition, values of $T_{min} > T_{max}$, values of T_{max} or T_{min} less than -50° C or greater than 55° C (i.e. outside historical bounds) were also replaced with the flag value (i.e. -9999). These steps were intended to screen out implausible values due to observer or data entry error, as well as misinterpretation of written data fields.
Finally, we assed the homogeneity of each primary station prior to further processing steps. We evaluated station history metadata to account for errors and discontinuities due to station moves throughout the record (Easterling et al., 1996; Peterson et al., 1998). If a station was found to change geographical position and this change was not large (< 10 km) we retained the station in the data set and corrected the coordinates to reflect the most current position; the occurrence of known station moves was less than 2% (3 out of 176). Thus all stations in the data set maintained one location for the entire record. In addition, the moves we could account for occurred in the early part of the record (<1960) and thus should not greatly influence trends, such as moves from urban to rural stations (Hansen et al., 2001).

Filling missing data

Estimates for missing data were generated with the multiple imputation (MI) procedure in the statistical program SAS (SAS Institute Inc., 2002). The MI procedure is a Monte Carlo technique in which missing values are replaced or "imputed" with several simulated values generated by stochastic modeling of the observed data variability (Rubin, 1987; Schafer, 1997; Levy, 1999). The imputed data sets are complete with observed non-missing data remaining unchanged while the original missing observations are replaced with new estimated values. This procedure produces data that can then be used with normal parametric statistics (Levy, 1999). MI has been utilized in a range of disciplines such as medical research (Barnard and Meng, 1999), public and occupational health (Zhou et al., 2001; Emenius et al., 2003), and more recently for environmental and global change sciences (Hui et al., 2004; Hanson et al., 2007). More detail on the multiple imputation technique for estimation of missing data can be found in Rubin, (1987) and Schafer, (1997), as well as Hui et al., (2004) for environmental monitoring and modeling purposes. There were approximately < 1% and < 1.5% missing or flagged observations for temperature and precipitation, respectively. The MI procedure was only used for brief periods of missing data (< 1 month) and imputed values were held within historical bounds. We used the median for each missing observation from the distribution of plausible values created using 1000 imputations. A final set of consistency checks were run on the filled data sets to ensure that the estimates did not violate obvious constraints associated with recording maximum and minimum temperatures, such as those described in the previous section.

Gridding Interpolation

Following all the preprocessing and data gap filling steps, the interpolation of daily climate data, from the relatively irregularly spaced station locations to the nodes of a regularly spaced grid, was accomplished using the Inverse Distance Weighting (IDW) spatial interpolation algorithm. The IDW procedure determines unknown cell values using a linear-weighted combination of included sample points within a specific neighborhood (Nalder and Wein, 1998; Bolstad, 2002); in this analysis we used the 12 nearest stations, which is common (Jarvis and Stuart, 2001). IDW interpolation explicitly implements the assumption of spatial autocorrelation, or objects that are closer together are more similar in character than those that are farther apart. Furthermore, IDW is an exact interpolator, whereby the interpolated surface passes through all points whose values are known (i.e. IDW honors the observed data points) and as such, the maximum and minimum values in each interpolated surface can only occur at the observed locations. Given this criterion, exact interpolation techniques tend to dampen extreme values at un-sampled locations, as is the case with IDW, but preserve the natural variability (i.e. roughness) in the data, which is important for preserving the spatial patterns in the data at a regional scale.

After an initial analysis of different spatial interpolation techniques (e.g. kriging, and smoothing splines) and due to the large, well dispersed station density throughout the data record, we determined IDW to be adequate to characterize the daily spatial patterns of both temperature and precipitation for this relatively low topographic complexity region. The final IDW grids were produced at 5' (8-km) latitude-longitude resolution using an automated procedure programmed using the object-oriented language ArcObjects in the Environmental Sciences Research Institute (ESRI) geographical information system software ArcGIS (version 9.2).

Once the interpolator (IDW) was chosen, we analyzed a subset of data to determine the optimum power parameter (n) to be use with the automated gridding of both temperature and precipitation; we used data covering all four of Wisconsin's meteorological seasons (i.e. winter, spring, summer, fall). The criteria for choosing the optimal n for the variables was a value that best minimized the mean bias and absolute errors (see validation section), plot as a function of the power value (data not shown), over an entire year; the mean error was given precedence if there was a disparity between this and the absolute errors. We chose a value of n equal to 1.1 for T_{max} and T_{min} and 2 for precipitation (P_{Total}) to preserve the broad patterns in temperature and local variation (i.e. spatial detail) in precipitation events.

Methodology of product validation

To evaluate the spatial coherence and overall accuracy of the interpolated climate surfaces, we used actual T_{max}, T_{min} and P_{Total} observations from the previously withheld stations to perform an independent validation. There were 104 withheld or validation stations available with sufficient observational record to be used in the validation, for the 1950 to 2006 period. Several stations had variable records (e.g. 5-49 years), but nonetheless provide an extremely useful test of our output climate grids; stations varied by climate division with a minimum of 9 to a maximum of 21. Furthermore, the number of stations and distribution is comparable to or better than other studies using withheld stations for validation (e.g. Price et al., 2000; Vicente-Serrano et al., 2003). The geographic locations for each station was used to extract a predicted value from each grid cell centroid for each surface (T_{max}, T_{min} and P_{Total}) and organized into a consistent time-series for comparison with the observed values at daily and monthly time-steps using the Starspan utility (Rueda et al., 2005). The performance of the IDW interpolated surfaces were then evaluated with two measures of efficiency with the mean error (ME) and mean absolute error (MAE).

The mean error provides an assessment of the trend in residuals or bias, either producing generally higher (i.e. over-prediction) or lower (i.e. under-prediction) values with respect to observations. The MAE is an absolute measure of the deviation of the predicted mean from the observed values at each validation station, ignoring its sign and thereby providing an indicator of the overall performance of the interpolator; high MAE's indicate poor prediction performance, while low MAE's suggest high confidence in the gridded values, such that the interpolated values reproduce the observations well (Daly, 2006; Willmott and Matsuura, 2006). We avoid using the root mean square error (RMSE) as this statistic generally inflates, often non-monotonically, the mean errors and thus provides an overly ambiguous measure of predicted surface accuracy, especially when error variance is large (Willmott and Matsuura, 2005; Willmott and Matsuura, 2006). We instead provide the standard deviation of signed errors (i.e. ME's) to evaluate the spread in the distribution of errors. In addition, we provide a subjective but nonetheless important analysis of the grid spatial representation with respect to known weather patterns using empirical knowledge of the climate in Wisconsin for evaluation (Daly et al., 2002). The evaluation of the climate surfaces allowed the assessment of (1) the realism and reasonableness of the spatial interpolated values and (2) the accuracy of the gridded values for unknown (i.e. validation) locations as the interpolation is essentially a prediction of values at locations for which physical data does not exist. Unless notes otherwise, all statistical tests were considered significant at $\alpha = 0.05$ level.

Appendix B: Snow Methodology

SNOW-17 is a conceptual snow accumulation and ablation model (Anderson, 1973, 2002, 2006), a component of the National Weather Service's River Forecast System (NWSRFS). This operational snow model explicitly treats most of the key physical processes that operate within a snow cover in a simplified manner, requiring only commonly available data observations of temperature and precipitation as inputs. In treating a column of snow, the model addresses the following principal processes: form of precipitation, accumulation of snow cover, energy exchange at the snow-air interface, heat exchange at the soil-snow interface, heat storage and deficit within the snowpack, internal state of the snow cover, and liquid water retention and transmission of water through the snow cover.

SNOW-17 uses air temperature as the sole index for estimating energy exchange at the snow-air interface. Air temperature is a reliable indicator of snowmelt and is a readily available observation. In addition, temperature is easily extrapolated across elevational gradients using lapse rates, which is critical since elevation is the main factor explaining temperature variance across a region, in addition to forest cover, slope, and aspect. Previous studies have shown that the typical temperature separating rain from snow is about 1.5°C (Snow Hydrology, 1956). SNOW-17 uses a single threshold temperature, specified by parameter PXTEMP, to diagnose the form of precipitation as snow (T<PXTEMP) or rain (T>PXTEMP).

SNOW-17 requires careful, regionally-specific calibration to produce quality snow simulation results. The model includes twelve key parameters, six of which are considered major parameters and can substantially effect the simulation; the allowable ranges for these parameters are specified by Anderson (2002). The following are the six major parameters:

1. SCF = snow correction factor, or gage catch deficiency adjustment factor
2. MFMAX = maximum melt factor, assumed to occur on June 21
3. MFMIN = minimum melt factor, assuming to occur on December 21
4. UADJ = average wind function factor for rain-on-snow periods
5. SI = maximum water equivalent, representing the water equivalent above which 100% snow cover exists
6. ADC = areal depletion curve, which consists of eleven values and determines the extent of snow cover versus bare ground in a region.

The six minor parameters are as follows:

1. MBASE = melt base temperature for snowmelt computations during non-rain periods
2. NMF = maximum negative melt factor, impacting heat gain or loss from snow pack
3. DAYGM = average daily ground melt, treated as a constant daily amount of melt which occurs at the snow-soil interface
4. PLWHC = percent liquid water-holding capacity for ripe snow
5. PXTEMP = rain-snow temperature index, used to assess the form of precipitation
6. TIPM = antecedent temperature index parameter, impacting energy exchange during non-melt periods.

In computing snow accumulation, the form of precipitation is determined by the threshold temperature, PXTEMP. The density of new snow is calculated as a function of temperature,

given that colder air masses tend to support less dense snow. Snow cover is modeled as a single, bulk layer with a specified water holding capacity. In determining the areal extent of snow cover, the areal depletion curve relates the areal snow extent to areal water equivalent based on the maximum water equivalent on record for a region and the water equivalent above which full snow cover exists. Snowmelt is calculated by a different set of equations for rain-on-snow and non-rain periods. For rain-on-snow events, energy and mass balance equations are applied, using the wind parameter UADJ. For non-rain periods, surface snowmelt is determined by temperature, using a melt factor with seasonal variations provided by a sine function using MFMAX for June 21 and MFMIN for December 21. Forest cover largely determines snowmelt rates, and thus Anderson (1996) recommends initial ranges for MFMAX and MFMIN based on forest cover types. SNOW-17 computes changes in snow density, necessary for calculating snow depth, due to compaction, destructive metamorphism, and melt metamorphism in response to the presence of liquid water.

Daily maximum and minimum temperature and daily precipitation from the WICCI gridded downscaled dataset for 1961-2000 from the 20C3M scenario is used to force the SNOW-17 model in multiple stages of calibration (Notaro *et al*., 2010b). The daily maximum and minimum temperature data is converted into hourly temperature data using an interpolatory spline under tension, assigning the minimum temperatures to 6Z and maximum temperatures to 18Z each day. Daily precipitation amounts are converted into hourly values by randomly distributing the precipitation on wet days into continuous six-hour periods, with the assumption that a typical precipitation event may last six hours. SNOW-17 output includes daily snowfall, snow depth, snow water equivalent in the snow pack, and snow cover fraction. To calibrate the model parameters, mean annual totals and the mean seasonal cycles of both snowfall and snow depth are compared between the 20C3M simulations of SNOW-17 and observations at 14 weather stations distributed across Wisconsin. These stations are a subset of 440 U.S. stations considered homogeneous and of highest quality by the plurality of seven expert judges in the study by Kunkel et al. (2009).

The following describes the choice in parameter values resulting from the calibration process. Regarding the temperature for distinguishing snow from rain events, Anderson (2002) states that PXTEMP=1.0°C should be adequate. This was investigated using hourly weather observations and temperature measurements for 1980-1999 from three distant Wisconsin locations, Milwaukee, Rhinelander, and LaCrosse, in the NCDC Global Surface Hourly database. For these stations, it is found that an equal likelihood of snow or rain consistently occurs around 1.3-1.4°C, so a value of PXTEMP=1.3°C is selected.

Given that snowmelt is sensitive to forest cover and type (Anderson, 1996, 2002; NWSRFS User's Manual), values of percent total tree (TREE), evergreen tree (EVE), and deciduous (DEC) tree cover are interpolated over the 0.1° x 0.1° grid using data from the Advanced Very High Resolution Radiometer (AVHRR) Continuous Fields Tree Cover Project (DeFries et al., 1998, 2000; Hansen et al., 2000). Similar to those recommended by Anderson (2002), the following values for MFMAX and MFMIN are applied, leading to favorable agreement with snow climatologies at the 14 calibration stations:

1. Bare or sparsely forested (TREE< 33%): MFMAX=1.7 mm/°C/6hr, MFMIN=0.4 mm/°C/6hr

2. Evergreen forest (TREE>33%, EVE-DEC>20%): MFMAX=0.5, MFMIN=0.2
3. Deciduous forest (TREE>33%, DEC-EVE>20%): MFMAX=1.1, MFMIN=0.1
4. Mixed forest (TREE>33%, |DEC-EVE|<20%): MFMAX=1.2, MFMIN=0.15

Snowmelt is most rapid in regions with minimal tree cover and is slowest within dense conifer forests, related to available sunlight at the surface.

The average wind function factor for rain-on-snow periods, UADJ, can be estimated by UADJ=0.002*U, where U is the 6-hourly wind travel in km at one meter above the snow surface (Anderson, 1976). A dataset of recommended UADJ values for the United States, created by Naoki Mizukami using a monthly 10-meter wind climatology from the North American Regional Reanalysis (Mesinger *et al*., 2006), is used to provide UADJ values for Wisconsin grid cells; values range from 0 to 0.04 mm/hPa, with forested areas experiencing lower wind speeds due to greater roughness (Anderson, 2002).

Elevation for each grid cell is retrieved from a topography dataset for the United States from GEON (geon.unavco.org); elevation is used to estimate atmospheric pressure, which affects the sensible heat flux calculations, a critical variable in the snow cover energy balance equation of SNOW-17. The areal depletion curve, labeled as "curve B" and identified as the most common curve in the NWSRFS User's Manual, is used for Wisconsin. Given that SNOW-17 is run for the entire state of Wisconsin, the snow correction factor, SCF, is set to 1, since it is impractical to assess the exposure of all weather stations in the state. The maximum water equivalent, SI, is assigned the value of 30 mm (typically equivalent to one foot of snow). As recommended by Anderson (2002), NMF=0.15 mm/°C/6hr, MBASE=0°C, and PLWHC=0.04. The antecedent temperature index parameter, TIPM, is specified as a function of latitude, ranging from 0.27 in southern Wisconsin to 0.12 in northern Wisconsin, to permit larger values of TIPM for regions with shallower snow covers (Anderson, 2002). Likewise, the average daily ground melt, DAYGM, is specified as a function of latitude, ranging from 0.1 mm/day in southern Wisconsin to 0 in northern Wisconsin, based on the recommendation from Anderson (2002) that DAYGM be assigned values close to zero if the soil is generally frozen under the snow. Finally, the value of the threshold density is set to 0.15 gm/cm^3, a value used in earlier versions of SNOW-17 (Anderson, 2006), which produced deeper, more favorable snow depths.

As previously mentioned, SNOW-17 is calibrated in its 20C3M simulations, each forced by one of fifteen CMIP3 global climate models, against climatological snowfall and snow depths data from 1961-2000 for fourteen Wisconsin weather stations in the Kunkel et al. (2009) database. Among these fourteen Wisconsin sites, the mean observed annual snowfall ranges from 103.2 cm (40.62 inches) at the southernmost station, Richland Center, to 159.4 cm (62.76 inches) at the northernmost station, St. Germain, with the likelihood of precipitation to fall in frozen form increasing with latitude and the gradual rise in elevation towards the north. A comparison of annual mean snowfall between SNOW-17 and observations at these fourteen sites yields a correlation of 0.77 ($p<0.01$), a root-mean-square-difference of 11.2 cm (4.4 inches), and a typical percent difference (defined as the mean of the absolute value of the differences) of 7.7%. Overall, there is good agreement between annual mean snowfall totals between SNOW-17 and observations, although there is a slight tendency for the model to produce too much snowfall.

Among the fourteen Wisconsin sites, the mean observed November-April snow depth ranges from 7.1 cm (2.79 inches) at Richland Center to 27.2 cm (10.70 inches) at St. Germain. A

comparison of mean November-April snow depth between SNOW-17 and observations, at these fourteen sites, results in a correlation of 0.86 ($p<0.01$), a root-mean-square-difference of 3.0 cm (1.2 inches), and a typical percent difference of 15.7%. Using one inch (2.54 cm) of snow depth as the criterion, the observed snow season across Wisconsin begins in mid-late November and ends in mid-March to mid-April.

There is a much greater variation among stations in the timing of the end of the snow season than the start of the snow season. In late autumn-early winter, a stochastic snow event can cover much of the state in snow, yet, in late winter-early spring, a cumulative period of warmth is necessary to melt away the present snow pack, particular in the northern Wisconsin sites. In comparing the simulated and observed snow season at the fourteen sites, the root-mean-square-differences for the mean start and end dates of the snow season are 5.6 and 5.8 days, respectively. Correlations between the model and observations at the fourteen sites for start date, end date, and duration of the snow season are 0.80, 0.89, and 0.86, respectively ($p<0.01$). The observed (simulated) snow season duration ranges from 16 (19) weeks at Richland Center to 22 (22) weeks at St. Germain. Overall, simulated and observed snow depths agree fairly well, although the duration of the simulated snow pack is too long and the simulated depth is typically too shallow, particularly for the northernmost sites like St. Germain.

Given the satisfactory agreement between observed and simulated snowfall and snow depth at the fourteen calibration sites, the aforementioned parameter values are used for an array of experiments, in which SNOW-17 is driven by downscaled gridded temperature and precipitation across the Wisconsin domain for the IPCC AR4 emission scenarios of 20C3M for the late 20th century and A2, A1B, and B1 for the mid- and late 21st century (Notaro *et al*., 2010b). Greenhouse gas emissions are largest with the A2 scenario and smallest with the B1 scenario by the end of this century. For all scenarios, downscaled output from 11-15 global circulation models is used to drive SNOW-17, using three realizations of temperature and precipitation from their PDFs for each model to produce an ensemble of potential snow projections.

Previously, observed snow data at fourteen homogeneous sites from the Kunkel et al. (2009) database were used to calibrate SNOW-17 across Wisconsin, leading to a favorable set of parameter values for the model and the creation of an extensive ensemble of modern and future simulations. The statewide performance of a calibrated SNOW-17 model is now compared to annual mean snowfall climatologies at 189 stations across Wisconsin from the NCDC State Snow Climatology and Extremes dataset. Comparisons are made between the model and observations both at the individual stations and on a grid, in which the observations are fit to the same 0.1° WICCI grid.

Spatially, the simulated and observed annual snowfall maps agree reasonably well, with a spatial correlation of 0.88 ($p<0.01$) for 1756 Wisconsin land grid cells. The Wisconsin mean snowfall is 128.5 cm (50.6 inches) in the model and 121.3 cm (47.8 inches) in the observations, with 6% too much snowfall simulated statewide. The largest simulated biases are about 20 cm too much snowfall along the southern edge of the state and 20 cm too little snowfall along the northern edge. The correlation between annual mean snowfall in the SNOW-17 simulations of 20C3M and the observations at the 189 stations is 0.80 ($p<0.01$); one notable bias is SNOW-17 produces too much snowfall at the sites with the least observed snowfall (in southern Wisconsin) and too little snowfall at the sites with the most observed snowfall (in northern Wisconsin). Overall,

both the calibration analysis at fourteen sites and the performance evaluation at 189 sites yield favorable comparisons of the SNOW-17 simulations with observations.

Appendix C: Potential Evapotranspiration Methodology

The Priestley-Taylor (1972) method for estimating potential evapotranspiration considers both temperature and a full surface radiation budget that incorporates atmospheric moisture content and its effect on incoming radiation. As temperature increases, so does available kinetic energy, which helps drive evapotranspiration. However, a moister atmosphere, evident by a lower diurnal temperature range, would reduce solar input to the surface and reduce potential evapotranspiration.

In order to compute daily irradiance at the top of the atmosphere, calculations of solar declination, earth-sun distance, and half-day length must first be completed. Solar declination in radians is computed as follows (Martin and McCutcheon, 1998):

$$\delta = \frac{23.45\pi}{180}\cos\left(\frac{2\pi}{365}(172 - J)\right)$$

where J is the day of the year. Solar declination is converted to degrees by multiplying by 57.3. The relative earth-sun distance, which varies from 0.984 in January to 1.016 in July, is calculated by (Martin and McCutcheon, 1998):

$$\left(\frac{d}{d'}\right) = 1 + 0.017\cos\left[\frac{2\pi(186 - J)}{365}\right]$$

where d' is the mean earth-sun distance and d is the actual earth-sun distance. The inverse of this d/d' ratio is applied later. The solar constant, S_o, equals 1367 W/m^2. The formula for half-day length in degrees, representing the time from solar noon to sunset, is (Gates, 2003):

$$h_s = \text{acos}\ (-\tan\phi\ \tan\delta)$$

ϕ is latitude in degrees. The number of daylight hours (h_{day}), ranging from about eight to fifteen hours for Wisconsin during the year, can be computed as h_s(degrees)/360*24*2. The equation for daily irradiance at the top of the atmosphere, Q_o, in MJ/m^2/day, is as follows (Gates, 1980; Bristow and Campbell, 1984; Gates, 2003):

$$Q_o = 86400 S_o \left(\frac{d'}{d}\right)^2 \left(\frac{h_s \sin\phi \sin\delta + \cos\phi \cos\delta \sinh_s}{\pi}\right)$$

Next, the psychometric "constant" must be computed. Following the approach of Lu *et al*. (2005), the atmospheric pressure, P, in kPa is estimated from a gridded elevation (EL in meters) dataset using the formula:

$$P = 101.3 - 0.01055*EL$$

The specific heat of moist air at constant pressure, C_p, equals 1013 J/kg/°C. The latent heat of vaporization, λ, in MJ/kg, is calculated as a function of daily mean temperature (°C), rather than as a simple constant (Lu *et al*., 2005), based on the equation:

$$\lambda = 2.501 - 0.002361\left(\overline{T}^{\circ}C\right)$$

The psychometric "constant", γ, is then computed as follows (Lu *et al*., 2005):

$$\gamma = \frac{C_p P}{0.622\lambda}$$

Atmospheric transmissivity, τ, is calculated by (Bristow and Campbell, 1984):

$$\tau = A\left[1 - \exp\left(-B\Delta T^{c}\right)\right]$$

The daily temperature range, ΔT, in °C is computed as the difference between the daily maximum and minimum temperatures. The diurnal temperature range serves as an indicator of the amount of radiation that is attenuated by the atmosphere. The transmissivity equation contains three constants, A, B, and C. From Meza and Varas (2000), the coefficient A, which sets the upper limit for transmissivity (cloud-free transmissivity), can be set to 0.7. In the transmissivity formula, $[1-\exp(-B\Delta T^{C}]$ represents the daily reduction of transmissivity mainly from cloud cover. Coefficient B, which varies seasonally, is computed from the monthly mean daily temperature range (ΔT in °C) as follows (Bristow and Campbell, 1984):

$$B = 0.036\exp\left(-0.154\overline{\Delta T}\right)$$

Bristow and Campbell (1984) recommend a value of 2.4 for coefficient C, but that value should be tuned for the region of study. Compared to Surface Radiation Budget (SRB) data from the National Climatic Data Center for Wisconsin, using A=0.7 (from Bristow and Campbell, 1984; Meza and Varas, 2000) and B as a function of ΔT, an ideal value of C=2.258 is determined for the domain.

The mean daily solar radiation at the surface, R_s, in MJ/m^2/day, is computed as the product of the atmospheric transmissivity and daily solar radiation at the top of the atmosphere (Bristow and Campbell, 1984; Goodin et al., 1999):

$$R_s = \tau * Q_o$$

Given that ρ is the surface albedo, the net daily solar radiation at a point on the Earth's surface, $R_{n,s}$, in W/m^2 is calculated by:

$$R_{n,s} = R_s\,(1-\rho)$$

From Kimball *et al*. (1997), a rough estimate of ρ=0.2 leads to $R_{n,s} \approx 0.8 * R_s$. However, in this study, a climatology of upward and downward shortwave fluxes at the surface, using SRB data, is applied to estimate the typical seasonal cycle of surface albedo for the Wisconsin domain, particularly since a surface albedo of 0.2 is too high. Over all land points (given that the spatial

differences are quite small), a seasonal cycle of surface albedo is used that ranges from 0.33 in mid-winter (snow-related) to 0.08-0.12 during the warm season depending on the presence of active vegetation. To summarize, the daily net solar radiation at the surface is estimated as a function of latitude, elevation, day of the year, surface albedo, and diurnal temperature range.

The rate of change of saturation vapor pressure with temperature is Δ, representing the slope of the saturation vapor pressure versus temperature curve. The slope, Δ in kPa/°C, is computed as a function of the daily mean temperature, T in °C as follows (Tetens, 1930; Murray, 1967):

$$\Delta = \frac{4098\left(0.6108e^{\frac{17.27T}{T+237.3}}\right)}{(T+237.3)^2}$$

The slope of the saturation vapor pressure-temperature curve increases roughly from 0.04 kPa/°C at 0°C to 0.26 kPa/°C at 30°C.

The Priestley-Taylor (1972) estimate of daily potential evapotranspiration, E_p in kg/m^2/s, is computed by this formula:

$$E_p = \alpha\left(\frac{\Delta}{\Delta+\gamma}\right)\left(\frac{R_n - G}{\lambda}\right)$$

R_n is the average daily net all-wave radiant energy flux, or net radiation, in W/m^2, and G is the average daily surface conductive energy flux, or soil heat flux, in W/m^2. In general, $G \approx 0.1 * R_n$ (Kimball *et al*., 1997). In the above potential evapotranspiration formula, Δ and γ have units of Pa/K. Priestley and Taylor (1972) recommend a coefficient α value of 1.26.

Since surface temperature was not available, Kimball *et al*. (1997) ignored the contribution of net thermal (longwave) radiation to the net all-wave radiation, meaning that R_n was approximately equal to the net solar radiation. For the WICCI study, all radiation fluxes are estimated rather than ignoring the longwave flux contributions. The methodology for estimating these radiation fluxes at the surface is explained below.

Clear sky atmospheric emissivity, ε_{ac} in W/m^2, is estimated from air temperature through an empirical relationship from Idso and Jackson (1969) that was considered "valid at any latitude and for any air temperature reached on earth," as follows:

$$\varepsilon_{ac} = 1 - 0.261 * \exp(-0.000777 * T^2)$$

The irradiance of a horizontal surface under clear skies at night can be approximated using surface air temperature, with a typical error of less than 5 W/m^2 using this empirical formula from Idso and Jackson (1969), which they considered valid for all latitudes and seasons. Surface emissivity, ε_s, is assigned the value of 0.96. Let $A = 1 - \varepsilon_{ac} / \varepsilon_s$. The total clear-sky radiation, Q_{TC} in MJ/m^2/day, is estimated as:

$$Q_{TC} = Q_o\ (-0.7 + 0.86 * h_{day})/h_{day}$$

If R_S (mean daily solar radiation at surface) is less than or equal to Q_{TC}, then assign the clear-sky ratio $R_c = R_S / Q_{TC}$. Otherwise, R_c is set to one.

The Stefan Boltzmann constant, σ, equals $5.67*10^{-8}$ W/m^2/K^4. Using the Stefan Boltzmann Law, with air temperature (T in °C) as a rough approximation for the unavailable surface temperature, the upward longwave radiation flux from the surface, R_{LU} in W/m^2, is estimated as:

$$R_{LU} = \varepsilon_s * \sigma * (273.15 + T)^4$$

The net longwave flux at the surface, R_{LN} in W/m^2, is computed as:

$$R_{LN} = A * R_{LU} * R_C$$

The downward longwave radiation flux at the surface, R_{LD} in W/m^2, is the difference between the upward and net longwave fluxes, as follows:

$$R_{LD} = R_{LU} - R_{LN}$$

This estimated net longwave flux at the surface is used to produce a more accurate estimate of the total net surface radiation flux, R_n, unlike in the study by Kimball *et al*. (1997) where the net longwave flux at the surface was ignored. A climatology of the upward and downward surface fluxes of both longwave and shortwave radiation is developed from these estimations from the WICCI data and compared to SRB data for 1984-2005. The close match for all radiation fluxes over Wisconsin helps validate the approach taken and estimations applied.

References

Alexander, L. V. X. Zhang, T. C. Peterson, J. Caesar, B. Gleason, A. M. G. Klein Tank, M. Haylock, D. Collins, B. Trewin, F. Rahimzadeh, A. Tagipour, K. Rupa Kumar, J. Revadekar, G. Griffiths, L. Vincent, D. B. Stephenson, J. Burn, E. Aguilar, M. Brunet, M. Taylor, M. New, P. Zhai, M. Rusticucci, J. L. Vazquez-Aguirre, 2006: Global observed changes in daily climate extremes of temperature and precipitation. *J. Geophysic. Res. – Atmos.*, **111**, DO5109, doi:10.1029/2005JD006290.

Anderson, E. A., 1973: National Weather Service River Forecast System-Snow Accumulation and Ablation Model. NOAA Technical Memorandum: NWS Hydro-17, US National Weather Service.

Anderson, E. A, 1976: A point energy and mass balance model of a snow cover. *NOAA Technical Report NWS,* **19**, 150 pp, February 1976.

Anderson, E., 1996: Initial parameter values for the snow accumulation and ablation model. NWSRFS User's Manual IV.2.2, <http://hsp.nws.noaa.gov/oh/hrl/nwsrfs/users_manual/htm/formats.htm>, 2001.

Anderson, E. A., 2002: Calibration of conceptual hydrologic models for use in river forecasting. Office of Hydrologic Development, US National Weather Service, Silver Spring, MD.

Anderson, E. A., 2006: Snow Accumulation and Ablation Model – SNOW 17. US Weather Service, Silver Spring, MD.

Armitage, A. M., 1997: Herbaceous Perennial Plants: A Treatise on their Identification Culture, and Garden Attributes. Stipes Publishing, L.L.C., Champaign, Illinois, 1141 pp.

Barnard, J. and Meng, X.L., 1999. Applications of multiple imputation in medical studies: From aids as nhanes. Stat. Meth. Med. Res. 8 (1), 17-36.

Bolstad, P., 2002. GIS fundamentals: A first text on geographic information systems. Eider Press, White Bear Lake, Minnesota, 412 pp.

Bristow, K. L., and G. S. Campbell, 1984: On the relationship between incoming solar radiation and daily maximum and minimum temperature. *Agric. For. Meteorol.*, **31**, 159-166.

Daly, C., 2006. Guidelines for assessing the suitability of spatial climate data sets. Int. J. Climatol. 26 (6), 707-721.

Daly, C., Gibson, W.P., Taylor, G.H., Johnson, G.L. and Pasteris, P., 2002. A knowledge-based approach to the statistical mapping of climate. Climate Res. 22 (2), 99-113.

DeFries, R. S., M. Hansen, J. R. G. Townshend, A. C. Janetos, and T. R. Loveland, 2000: A global 1-km dataset of percent tree cover derived from remote sensing. *Global Change,* **6**, 247-254.

DeFries, R., M. Hansen, J. R. G. Townshend, and R. Sholberg, 1998: Global land cover classifications at 8km spatial resolution: The use of training data derived from Landsat imagery in decision tree classifiers. *International Journal of Remote Sensing,* **19**, 3141-3168.

Easterling, D.R., Peterson, T.C. and Karl, T.R., 1996. On the development and use of homogenized climate datasets. J. Climate 9 (6), 1429-1434.

Emenius, G., Pershagen, G., Berglind, N. et al., 2003. NO_2, as a marker of air pollution, and recurrent wheezing in children: A nested case-control study within the BAMSE birth cohort. Occ. Environ. Med. 60 (11), 876-881.

Gates, D. M., 1980: Biophysical ecology. Springer-Verlag, New York.

Gates, D. M., 2003: Biophysical ecology. Springer-Verlag, New York.

Goodin, D. G., J. M. S. Hutchinson, R. L. Vanderlip, and M. C. Knapp, 1999: Estimating irradiance for crop modeling using daily air temperature data. *Agron. J.*, **91**, 845-851.

Groisman, P. Y., R. W. Knight, and T. R. Karl, 2001: Heavy precipitation and high streamflow in the continguous United States: trends in the 20th century. *Bull. Am. Met. Soc.*, **82**, 219-246.

Groisman, P. Y., R.W. Knight, T.R. Karl, D.R. Easterling, B. Sun, and J. H. Lawrence, 2004: Contemporary Changes of the Hydrological Cycle over the Contiguous United States: Trends Derived from *in situ* Observations. *Journal of Hydrometeorology,* 5, 64-85

Groisman, P. Y., R.W. Knight, D.R. Easterling, T.R. Karl, , G.C. Hegerl, and V.N. Razuvaev, 2005: Trends in intense precipitation in the climate record. *J. Climate*, **18**, 1326-1350.

Hansen, J., Ruedy, R., Sato, M. et al., 2001. A closer look at United States and global surface temperature change. J. Geophys. Res.-Atmos. 106 (D20), 23947-23963.

Hansen, M., R. DeFries, J. R. G. Townshend, and R. Sohlberg, 2000: Global land cover classification at 1km resolution using a decision tree classifier. *International Journal of Remote Sensing,* **21**, 1331-1365.

Hanson, P.C., Carpenter, S.R., Cardille, J.A., Coe, M.T. and Winslow, L.A., 2007. Small lakes dominate a random sample of regional lake characteristics. Fresh. Biol. 52 (5), 814-822.

Holman, K., 2010: M.S. Thesis, in preparation.

Hui, D.F., Wan, S.Q., Su, B. et al., 2004. Gap-filling missing data in eddy covariance measurements using multiple imputation (mi) for annual estimations. Agric. For. Meteorol. 121 (1-2), 93-111.

Idso, S. B. and R. D. Jackson, 1969: Thermal radiation from the atmosphere. *J. Geophys. Res.*, **74**, 5397-5403.

Jarvis, C.H. and Stuart, N., 2001. A comparison among strategies for interpolating maximum and minimum daily air temperatures. Part II: The interaction between number of guiding variables and the type of interpolation method. J. of App. Meteorol. 40 (6), 1075-1084.

Karl, T. R., G. A. Meehl, C. D. Miller, S. J. Hassol, A. M. Waple, and W. L. Murray, Eds., 2008: *Weather and Climate Extremes in a Changing Climate; Regions of Focus: North America, Hawaii, Caribbean, and U. S. Pacific Islands*. Synthesis and Assessment Product 3.3. Report by the U. S. Climate Change Science Program and the Subcommittee on Global Change Research. 180 pp.

Karl, T. R., Melillo, J. M., and Peterson, T. C., 2009: *Global Climate Change Impacts in the United States*. New York, NY: Cambridge University Press.

Kimball, J. S., S. W. Running, and R. Nemani, 1997: An improved method for estimating surface humidity from daily minimum temperature. *Agric. For. Meteorol.*, **85**, 87-98.

Kucharik, C. J., S. P. Serbin, E. J. Hopkins, S. Vavrus, and M. M. Motew, 2010: Patterns of climate change across Wisconsin from 1950 to 2006. *Physical Geography*, **31**, 1-28.

Kunkel, K.E., D. R. Easterling, K. Redmond, and K. Hubbard, 2003: Temporal Variations of Extreme Precipitation Events in the United States: 1895-2000. *Geophysical Research Letters*, **30**, doi:10.1029/2003GL018052, 2003.

Kunkel, K.E., X.-Z. Liang, J. Zhu, and Y. Lin, 2006: Can CGCMs simulate the Twentieth Century "warming hole" in the central United States. J. Climate, 19, 4137–4153.

Kunkel, K. E., M. Palecki, L. Ensor, K. G. Hubbard, D. Robinson, K. Redmond, and D. Easterling, 2009: Trends in twentieth-century U.S. snowfall using a quality-controlled dataset. *Journal of Atmospheric and Oceanic Technology,* **26**, 33-44.

Kunkel, K., R. Pielke Jr., S. Changnon, 1999: Temporal fluctuations in weather and climate extremes that cause economic and human health impacts. *Bull. Am. Meteorol. Soc.*, **80**, 1077-1098.

Levy, P.S., 1999. Sampling of populations: Methods and applications. Wiley, New York.

Lu, J., G. Sun, S. G. McNulty, and D. M. Amatya, 2005: A comparison of six potential evapotranspiration methods for regional use in the Southeastern United States. *Journal of the American Water Resources Association*, June 2005, 621-633.

Madsen, T., 2007: When it rains, it pours: global warming and the rising frequency of extreme precipitation in the United States. Boston, MA: Environment America Research and Policy Center. 48 pp.

Martin, J. L., and S.C. McCutcheon, 1999: Hydrodynamics and transport for water quality modeling. In: J. L. Martin and S. C. McCutcheon, Editors, Hydrodynamics and transport for water quality modeling, CRC Press, Boca Raton, FL, USA.

Meehl, G. A., C. Covey, T. Delworth, M. Latif, B. McAvaney, J. F. B. Mitchell, R. J. Stouffer, and K. E. Taylor, 2007: The WCRP CMIP3 multi-model dataset: A new era in climate change research. *Bulletin of the American Meteorological Society,* **88**, 1383-1394.

Meehl, G.A., Stocker, T.F., Collins, W.D., Friedlingstein, P., Gaye, A.T., Gregory, J.M., Kitoh, A., Knutti, R., Murphy, J. M., Noda, A., Raper, S.C.B., Watterson, I.G., Weaver, A.J., Z.-C. Zhao, Z.-C. 2007. Global climate projections. In: Solomon, S., D. Qin, M. Manning, Z. Chen, M. Marquis, K.B. Averyt, M. Tignor and H.L. Miller (Eds.), *Climate Change 2007: the Physical Science Basis*. Contribution of Working Group I to the Fourth Assessment Report of the Intergovernmental Panel on Climate Change, Cambridge University Press, Cambridge, and New York. pp. 747-845.

Mesinger, F., and Coauthors, 2006: North American Regional Reanalysis. *Bull. Amer. Meteor. Soc*, **87**, 343–360.

Meza, F., and E. Varas, 2000: Estimation of mean monthly solar global radiation as a function of temperature. *Agricultural and Forest Mereorology*, **100**, 231-241.

Moran, J.M. and Hopkins, E.J., 2002. Wisconsin's weather and climate. The University of Wisconsin Press, Madison, Wisconsin, 321 pp.

Murray, F. W., 1967: On the computation of saturation vapor pressure. *J. Appl. Meteor.*, **6**, 203 204.

Nakicenovic, N. et al (2000). *Special Report on Emissions Scenarios: A Special Report of Working Group III of the Intergovernmental Panel on Climate Change*, Cambridge University Press, Cambridge, U.K., 599 pp. Available online at: http://www.grida.no/climate/ipcc/emission/index.htm

Nalder, I.A. and Wein, R.W., 1998. Spatial interpolation of climatic normals: Test of a new method in the Canadian boreal forest. Agric. For. Meteorol. 92 (4), 211-225.

National Weather Service. NWSRFS User's Manual Documentation. http://www.nws.noaa.gov/oh/hrl/nwsrfs/users_manual/htm/xrfsdocpdf.php

Notaro, M., D. Lorenz, and D. Vimont, 2010a: 21st century Wisconsin gardening – Transformed by climate change. *Wisconsin Natural Resources*, submitted.

Notaro, M., D. Lorenz, D. Vimont, and S. Vavrus, 2010b: 21st century Wisconsin snow projections based on an operational snow model driven by statistically downscaled climate data. *International Journal of Climatology*, submitted.

Peterson, T.C., Easterling, D.R., Karl, T.R. et al., 1998. Homogeneity adjustments of in situ atmospheric climate data: A review. Int. J. Climatol. 18 (13), 1493-1517.

Price, D.T., McKenney, D.W., Nalder, I.A., Hutchinson, M.F. and Kesteven, J.L., 2000. A comparison of two statistical methods for spatial interpolation of Canadian monthly mean climate data. Agric. For. Meteorol. 101 (2-3), 81-94.

Priestley, C. H. B., and R. J. Taylor, 1972: On the assessment of surface heat flux and evaporation using large-scale parameters. *Mon. Weather Rev.*, **100**, 81-82.

Raupach, M., Marland, G., Ciais, P., Le Quere, C., Canadell, J., Klepper, G., et al. (2007). Global and regional drivers of accelerating CO2 emissions. *Proceedings Of The National Academy Of Sciences Of The United States Of America , 104* (24), 10288-10293.

Rubin, D.B., 1987. Multiple imputation for nonresponse in surveys. John Wiley & Sons, Inc., New York.

Rueda, C.A., Greenberg, J.A. and Ustin, S.L., 2005. Starspan: A tool for fast selective pixel extraction from remotely sensed data. Center for Spatial Technologies and Remote Sensing, University of California at Davis, Davis, CA.

Schafer, J.L., 1997. Analysis of incomplete multivariate data. Chapman and Hall, New York.

Schuster Z., and K. Potter, 2010: (internal citation to the Stormwater Working Group report).

Serbin, S.P. and C.J. Kucharik (2009). Spatio-temporal mapping of daily temperature and precipitation for the development of a multi-decadal climatic dataset for Wisconsin. Journal of Applied Meteorology and Climatology 48, 742-757.

Snow Hydrology. Summary Report of the Snow Investigations, North Pacific Division, Corps of Engineers, Portland, Oregon, 437 pp, June 1956.

Tetens, V. O., 1930: Uber einige meteorologische. Begriffe, *Zeitschrift fur Geophysik*. **6**, 297-309.

Trenberth, K. E., 1999: Conceptual framework for changes of extremes of the hydrological cycle with climate change. *Climatic Change*, 42, 327-339.

Vavrus, S., J. E. Walsh, W. L. Chapman, and D. Portis, 2006: The behavior of extreme cold-air outbreaks under greenhouse warming. *International Journal of Climatology*, 26, 1133-1147.

Vicente-Serrano, S.M., Saz-Sanchez, M.A. and Cuadrat, J.M., 2003. Comparative analysis of interpolation methods in the middle Ebro Valley (Spain): Application to annual precipitation and temperature. Climate Res. 24 (2), 161-180.

Willmott, C.J. and Matsuura, K., 2005. Advantages of the mean absolute error (MAE) over the root mean square error (RMSE) in assessing average model performance. Climate Res. 30 (1), 79-82.

Willmott, C.J. and Matsuura, K., 2006. On the use of dimensioned measures of error to evaluate the performance of spatial interpolators. Intern. J. Geog. Inf. Sci. 20 (1), 89-102.

Zhou, X.H., Eckert, G.J. and Tierney, W.M., 2001. Multiple imputation in public health research. Stat. Med. 20 (9-10), 1541-1549.

Figures

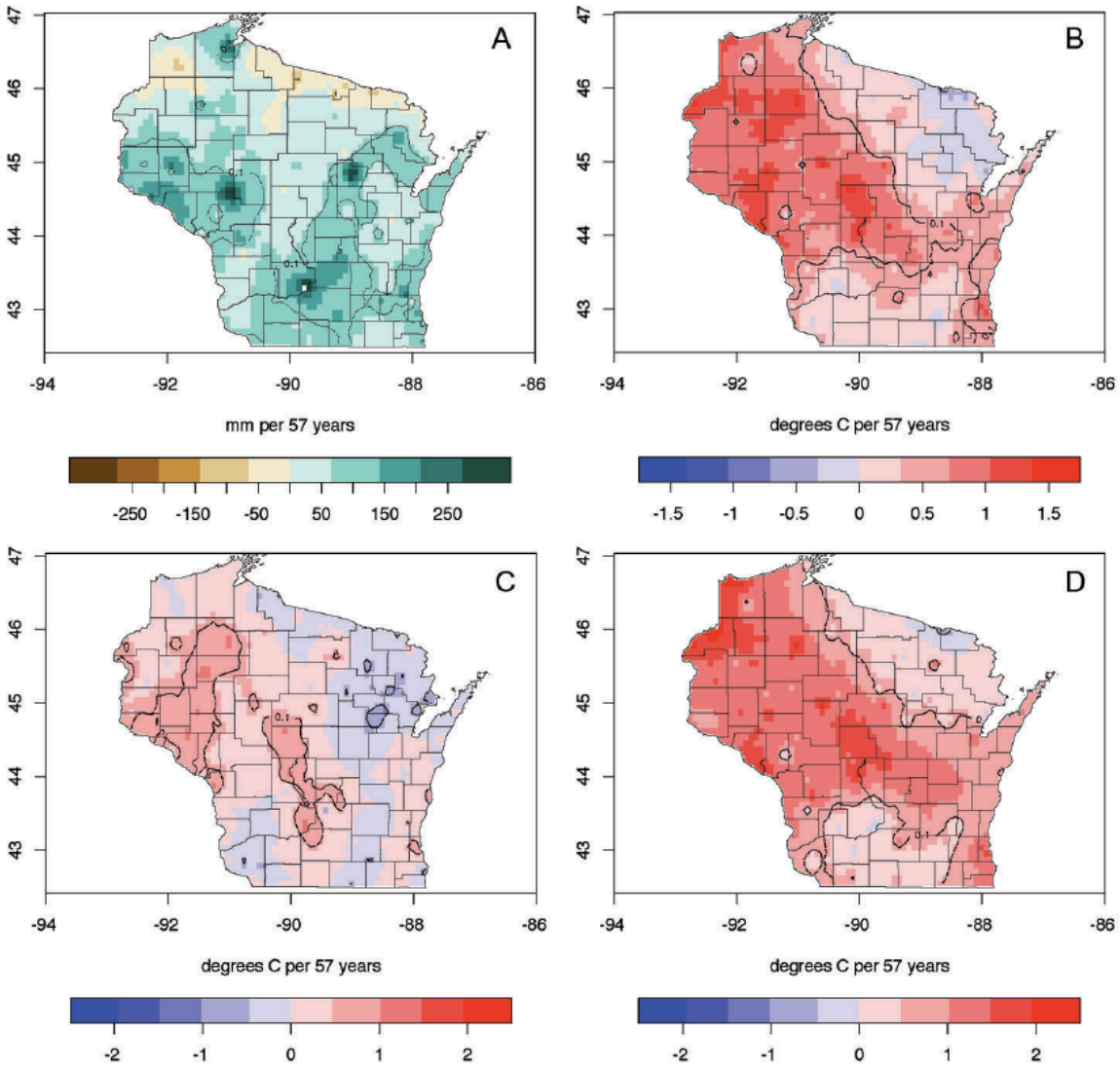

Figure 1: *(From Kucharik et al., 2010)* Trends from 1950 to 2006 in (A) total annual precipitation, (B) annual average temperature, (C) annual average maximum temperature, and (D) annual average minimum temperature. Regions that had statistically significant ($p > 0.1$) trends are enclosed or bounded by dark dashed lines.

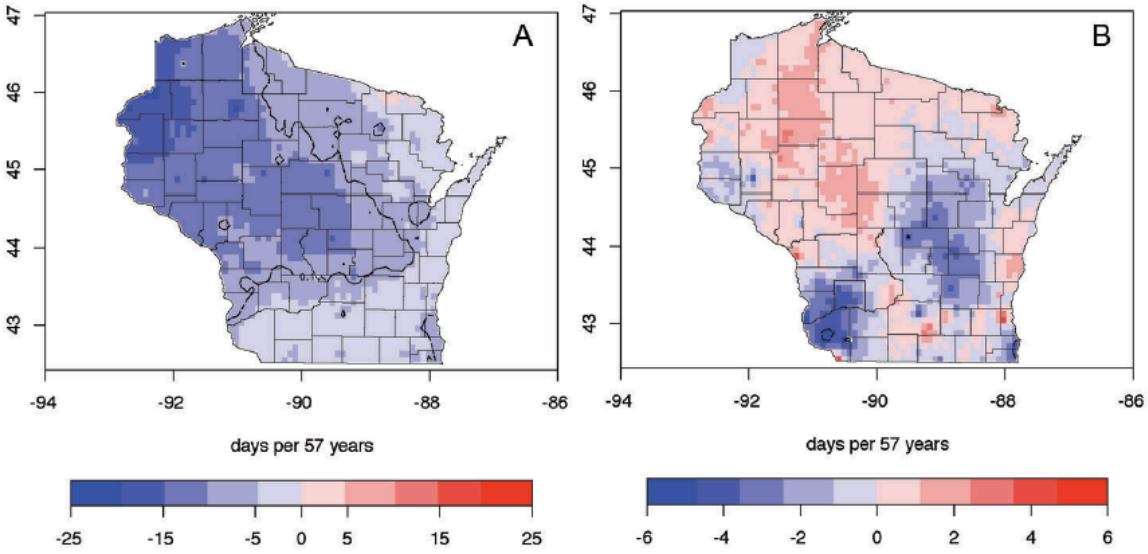

Figure 2: *(From Kucharik et al., 2010)*: Trends from 1950 to 2006 for the annual occurrence of daily temperatures (A) less than –17.8º C (0.0º F), and (B) greater than 32.2º C (90º F). Regions that had statistically significant ($p > 0.1$) trends are enclosed or bounded by dark dashed lines.

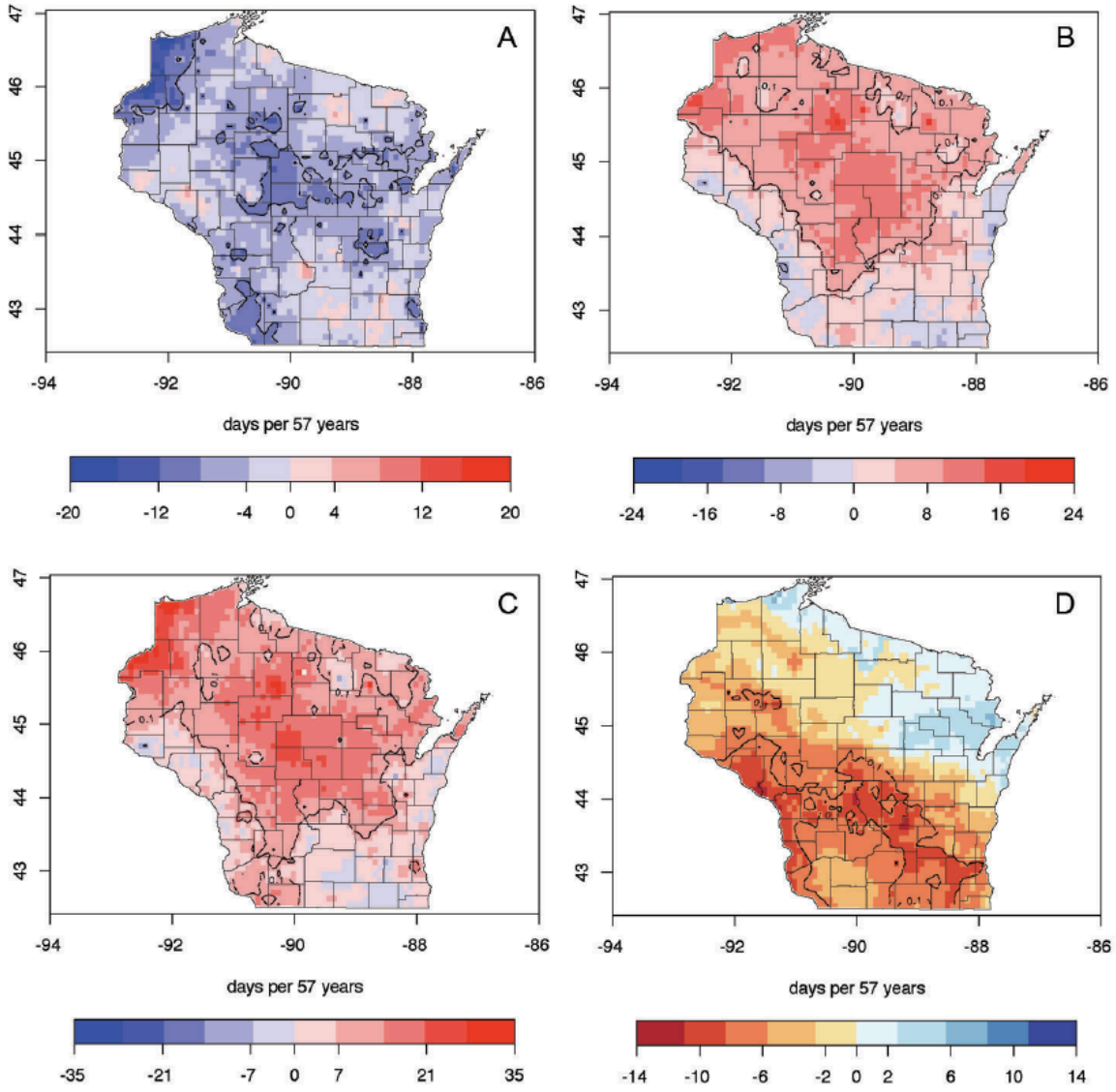

Figure 3: *(From Kucharik et al., 2010)* Trends from 1950 to 2006 for changes in (A) date of last spring freeze (threshold 0.0° C), (B) date of first fall freeze (threshold 0.0° C), (C) growing-season length (days between last spring freeze and first fall freeze), and (D) date of onset of spring (when 10-day running mean daily temperature reaches 10° C or 50° F). Regions that had statistically significant ($p > 0.1$) trends are enclosed or bounded by dashed lines.

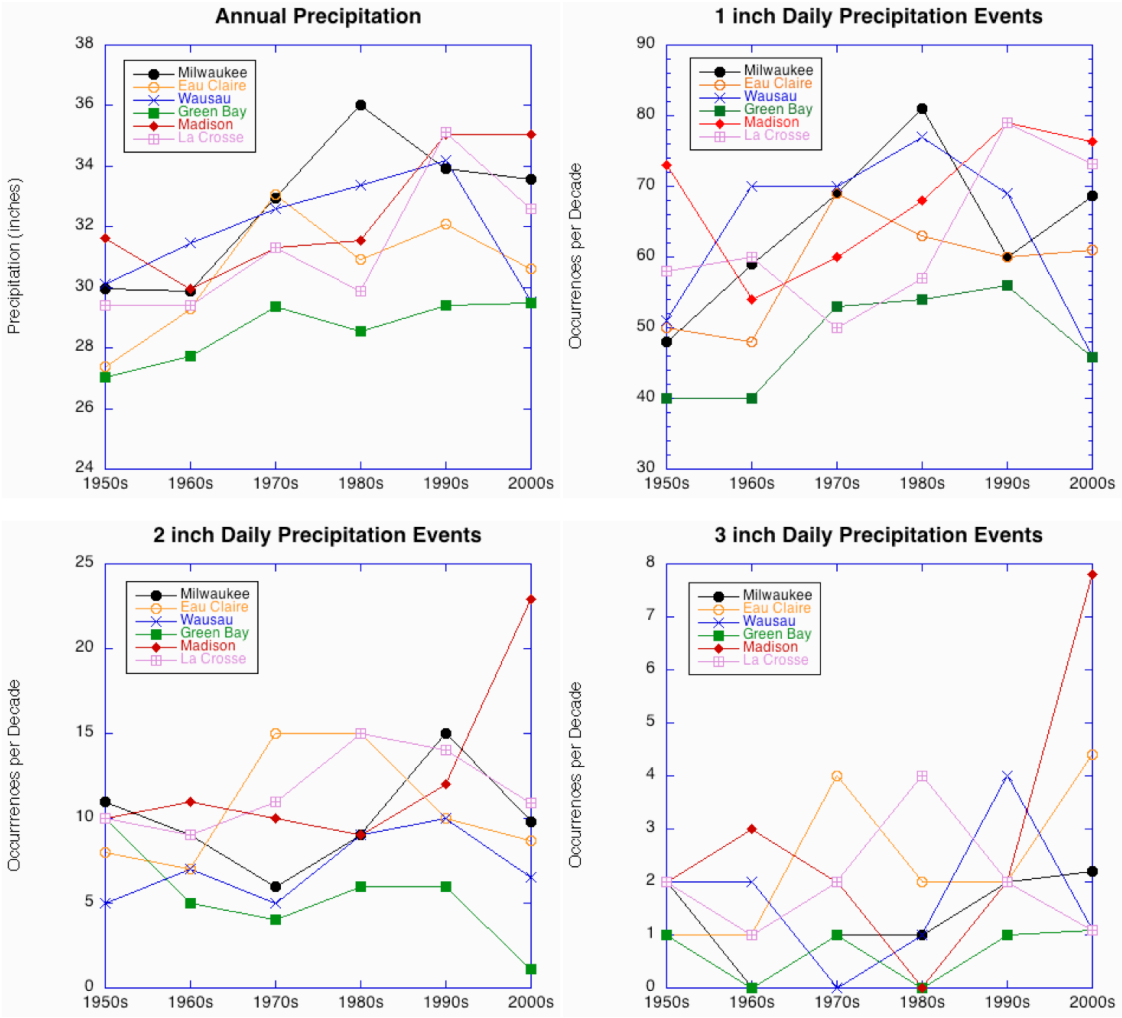

Figure 4: *(From Kucharik et al., 2010)* Annual and extreme precipitation at six first-order weather stations in Wisconsin from 1950-2008. The 2000s decade was adjusted upward by 11% to account for the missing 2009 year.

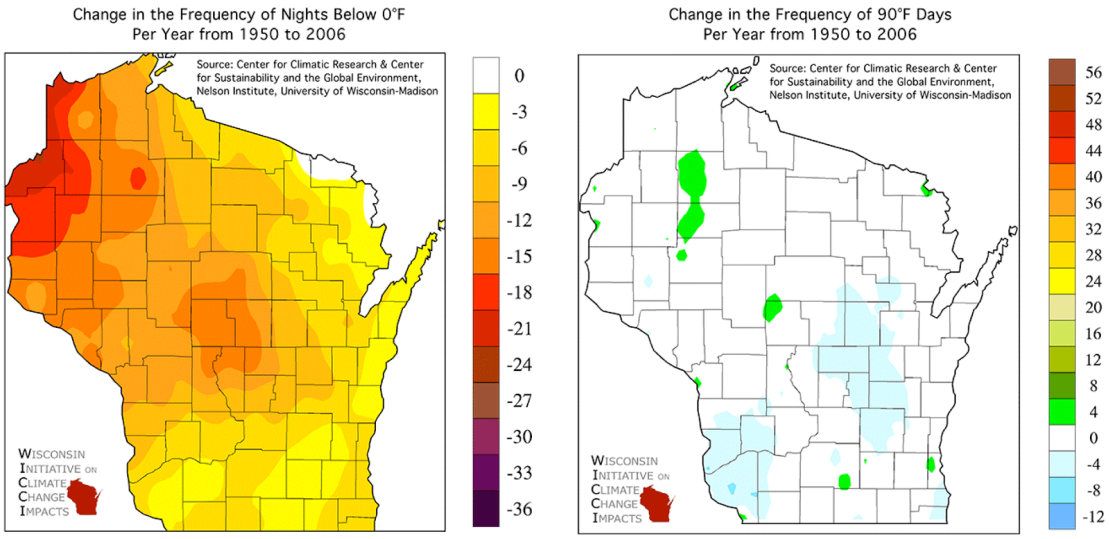

Figure 5: *(Adapted from Kucharik et al., 2010)* Observed trends in extreme heat and cold between 1950 and 2006. Daily minimum temperature below 0ºF [left], daily maximum temperature above 90ºF [right].

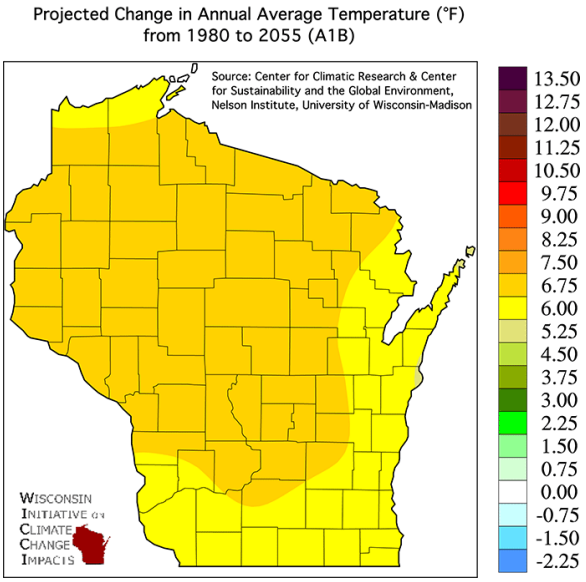

Figure 6: Projected warming for Wisconsin by the mid-21st century under the A1B scenario in °F. The map represents the average over all downscaled model projections.

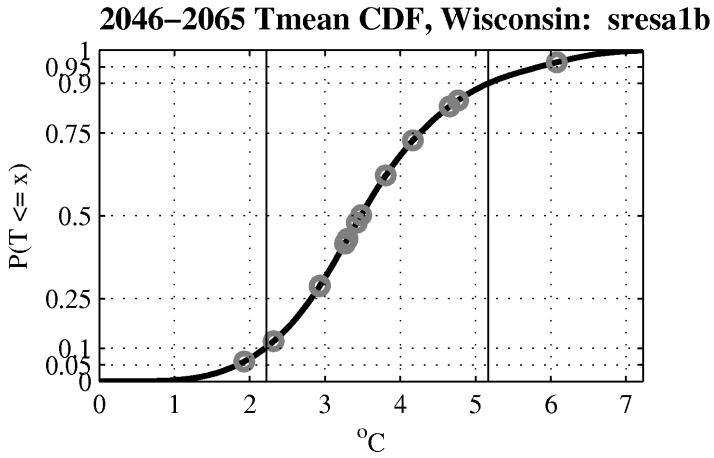

Figure 7. Cumulative probability distribution function (CDF) for projected annual average mean temperature change in Wisconsin estimated across all downscaled models. The solid line is the estimated PDF, and grey circles indicate the expected warming from each of the downscaled model projections. Vertical lines are drawn at the 10th and 90th percentiles.

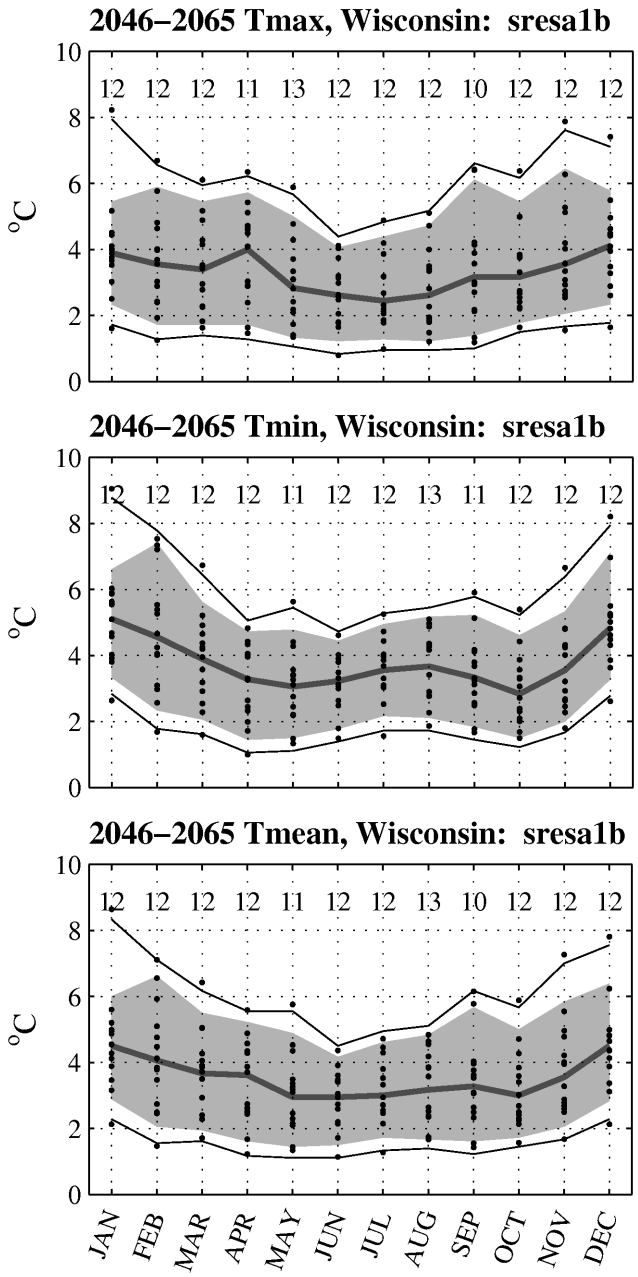

Figure 8. Cumulative probability distribution over all downscaled model projections for Wisconsin-mean daily mean (top), maximum (middle), and minimum (bottom) temperature under the A1B scenario, for mid-21st century conditions, and for each month of the year. For each panel, the thick grey line indicates the median temperature change across all models, the grey shading spans the 10th to 90th percentile, and the thin solid lines indicate the 5th to 95th percentiles. Black dots indicate individual model changes, and the numbers across the top indicate the number of models (out of 13) that fall within the 10th to 90th percentile (note that this usually exceeds 80% of the models due to our choice of kernel width in the kernel density estimator).

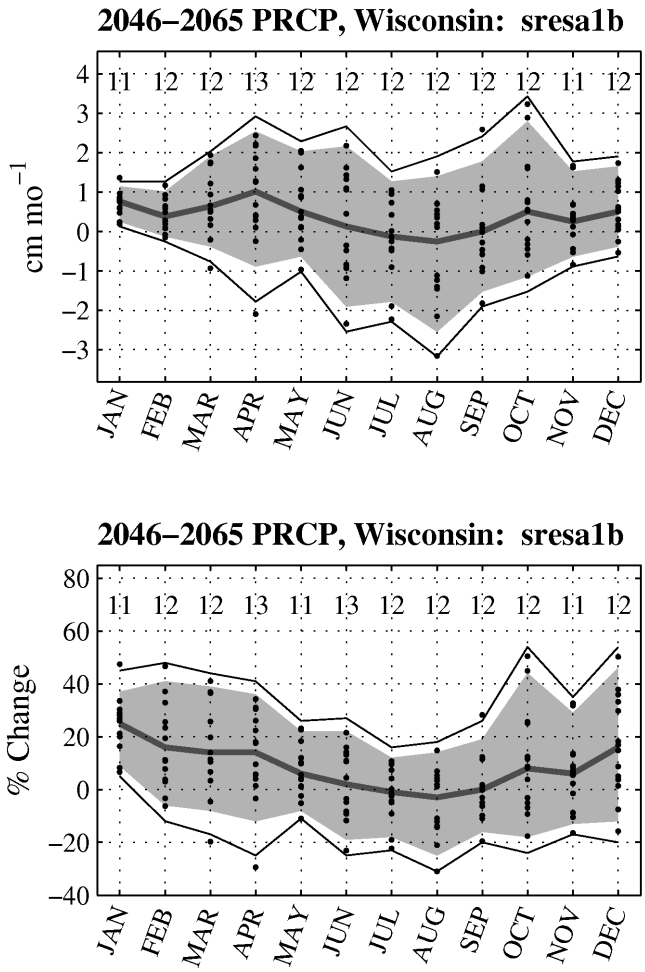

Figure 9. Cumulative probability distribution over all downscaled model projections for Wisconsin-mean raw monthly mean precipitation change (top; cm mo^{-1}) and for the percent change in precipitation (bottom; %), under the A1B scenario, for mid-21st century conditions, and for each month of the year. For each panel, the thick grey line indicates the median change across all models, the grey shading spans the 10th to 90th percentile, and the thin solid lines indicate the 5th to 95th percentiles. Black dots indicate individual model changes, and the numbers across the top indicate the number of models (out of 13) that fall within the 10th to 90th percentile (note that this usually exceeds 80% of the models due to our choice of kernel width in the kernel density estimator).

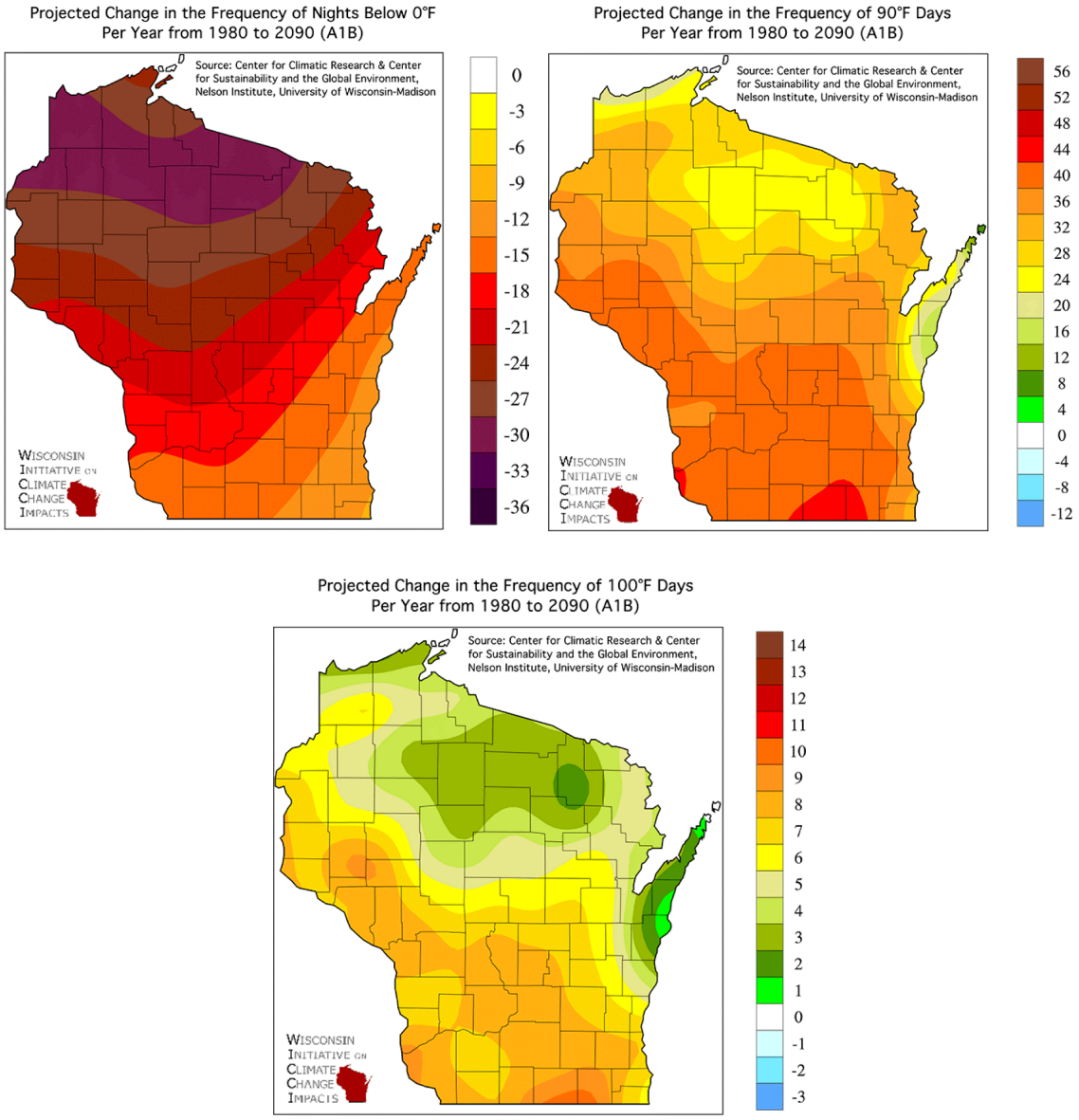

Figure 10. Projected future changes in the frequency of extreme temperatures in Wisconsin for the A1B emissions scenario during years 2081-2100 vs. 1961-2000. Daily minimum temperature below 0ºF [top left], daily maximum temperature above 90ºF [top right], daily maximum temperature above 100ºF [bottom].

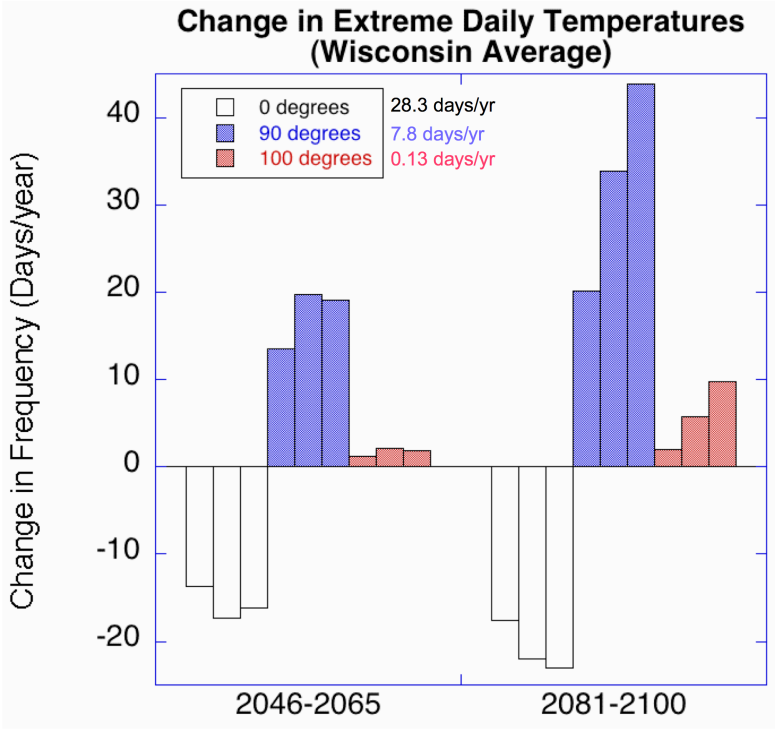

Figure 11. Projected future changes from the baseline period (1961-2000) in the annual frequency of extreme temperatures areally averaged over Wisconsin for the middle 21st century (2046-2065) and late 21st century (2081-2100). Daily minimum temperature below 0ºF (open bars), daily maximum temperature above 90ºF (blue), daily maximum temperature above 100ºF (red). The set of three bars for each time period represents the change for the B1, A1B, and A2 scenarios from left to right. The frequency of the extremes during the 20th century baseline period is listed next to the legend.

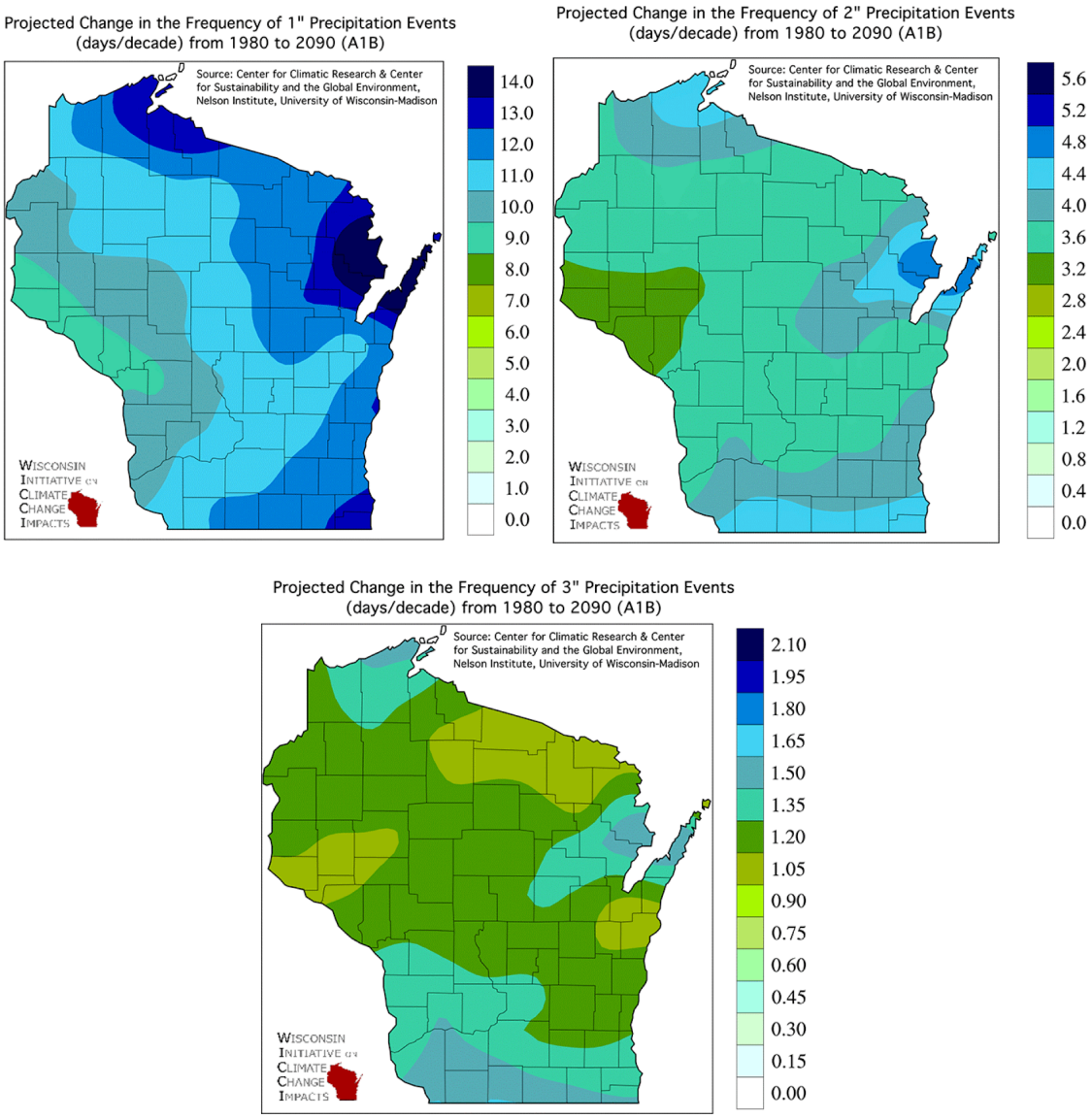

Figure 12. Like Figure 10 but for daily precipitation amounts of at least 1 inch [top left], 2 inches [top right], and 3 inches [bottom].

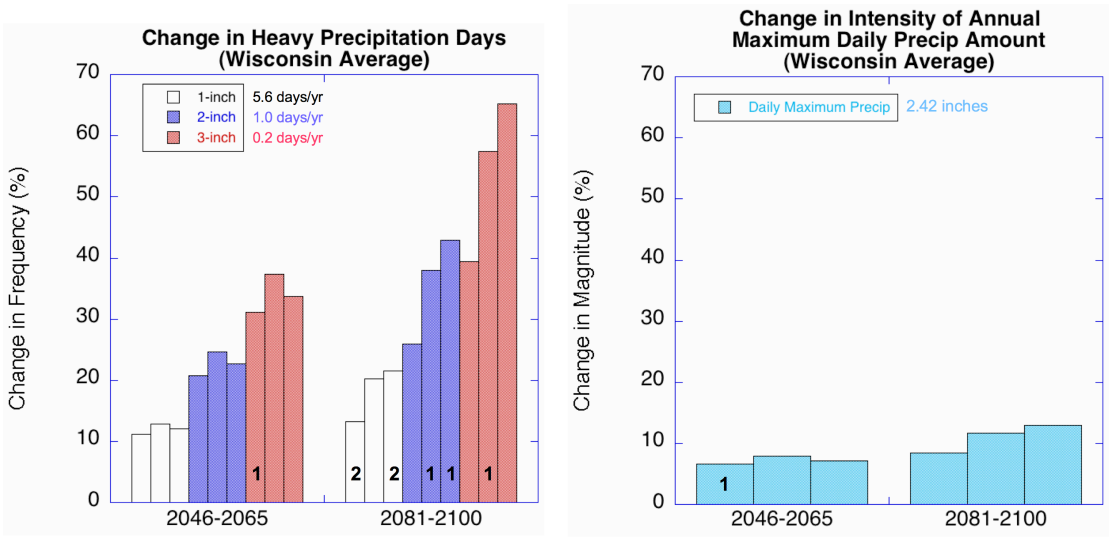

Figure 13: Like Figure 3 but for [left] *frequency* of extreme daily precipitation amounts---1 inch (open bars), 2 inches (blue), and 3 inches (red)---and [right] *intensity* of extreme precipitation, expressed as the average annual maximum of daily precipitation. The numbers inside the bars indicate the number of climate models that did not simulate an increase for a given scenario and time period, so the absence of a number means unanimous agreement among the models in the projected sign of the change.

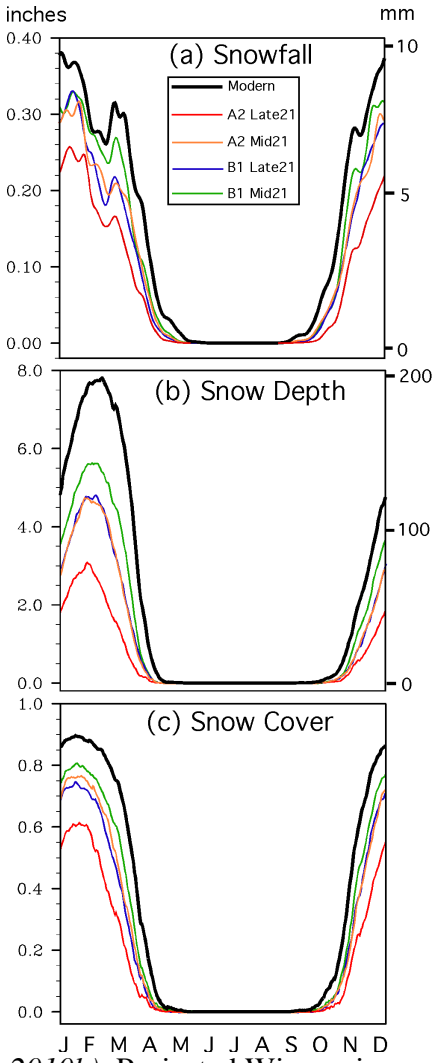

Figure 14. *(From Notaro et al., 2010b)* Projected Wisconsin-averaged (a) snowfall, (b) snow depth, and (c) snow cover, in both inches and mm, for "modern" (late 20th century – black), mid-21st century for B1 (green) and A2 (orange) scenarios, and late 21st century for B1 (blue) and A2 (red) scenarios, as simulated by SNOW-17.

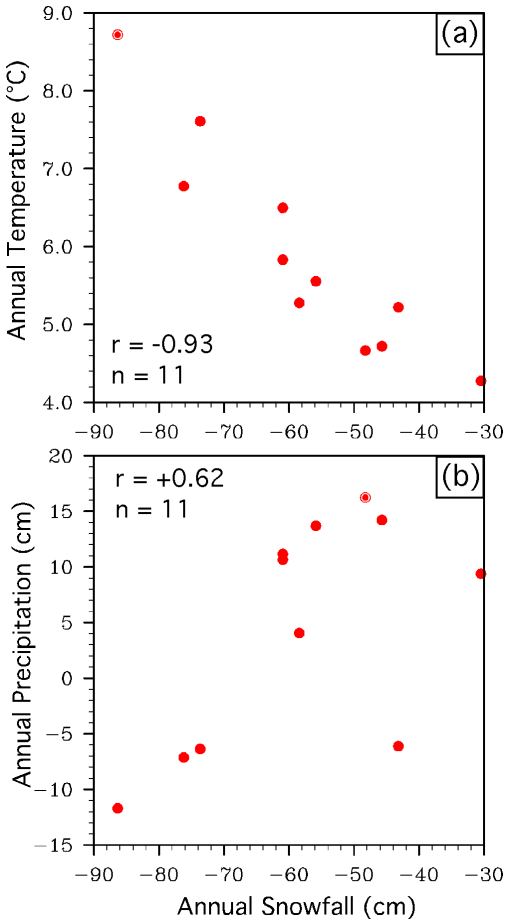

Figure 15. *(From Notaro et al. 2010b)* (a) Scatter plot of the projected changes in Wisconsin-averaged annual temperature (°C) and annual snowfall (cm), based on comparing the late 21st century under the A2 scenario with the late 20th century under the 20C3M scenario. Each individual dot represents a CMIP3 (Climate Model Intercomparison Project Phase Three) GCM (global climate model). (b) Same as (a), except comparing projected changes in annual precipitation (cm) and annual snowfall.

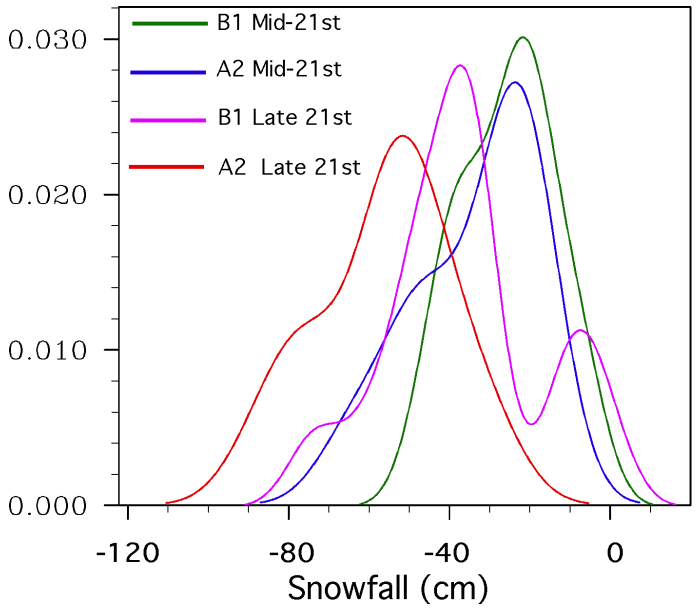

Figure 16. Projected change in Wisconsin's annual mean snowfall (cm) for the mid-21st (2046-2065) and late 21st century (2081-2100) using the A2 and B1 emission scenarios, based on SNOW-17 simulations. Results are shown as probability density functions using kernel density estimates. The range of projections (10th to 90th percentiles) for the mid-21st century is –9 to -42 cm for B1 and -14 to -58 cm for A2. For the late 21st century, the range is -8 to -62 cm for B1 and -35 to -83 cm for A2.

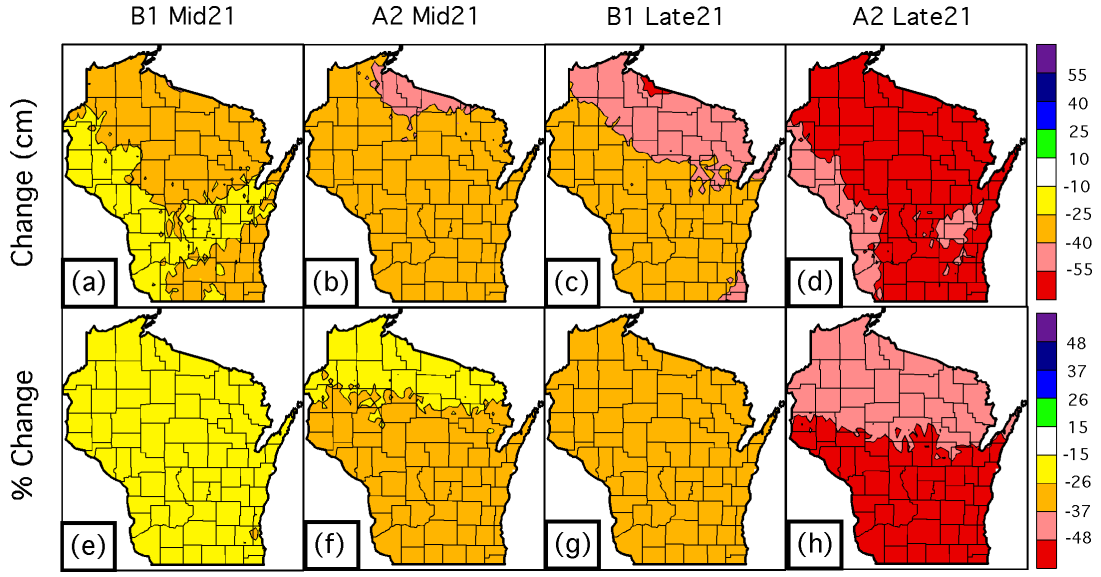

Figure 17. Projected changes in mean snowfall, shown as (a-d) absolute differences (cm) and (e-h) percent differences. Differences are based on comparing the late 20th century simulations from 20C3M with both mid- and late 21st century simulations for scenarios B1 and A2.

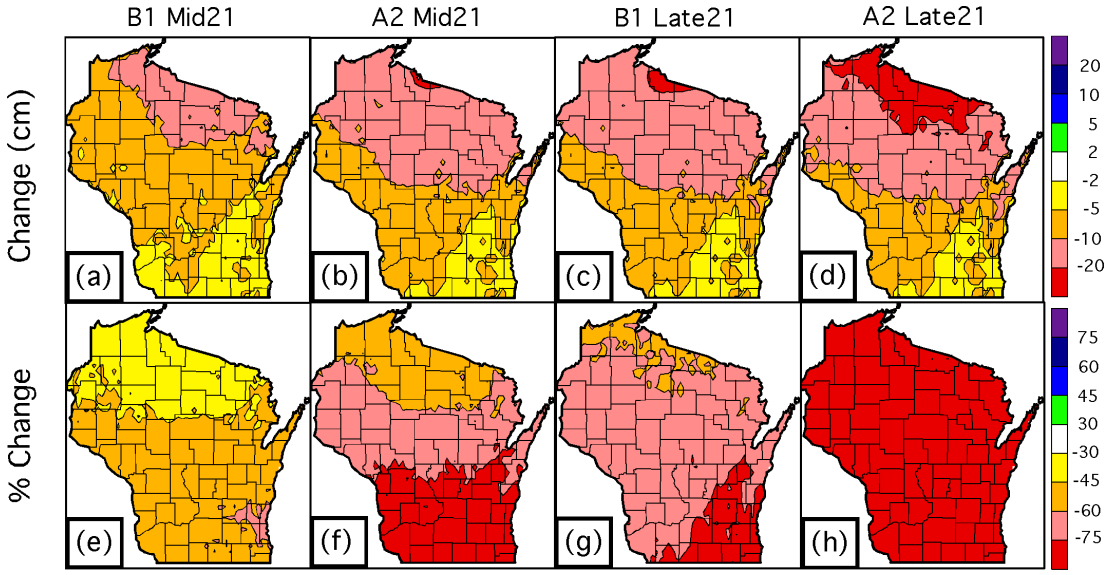

Figure 18. Projected changes in mean March 15th snow depth, shown as (a-d) absolute differences (cm) and (e-h) percent differences. Differences are based on comparing the late 20th century simulations from 20C3M with both mid- and late 21st century simulations for scenarios B1 and A2.

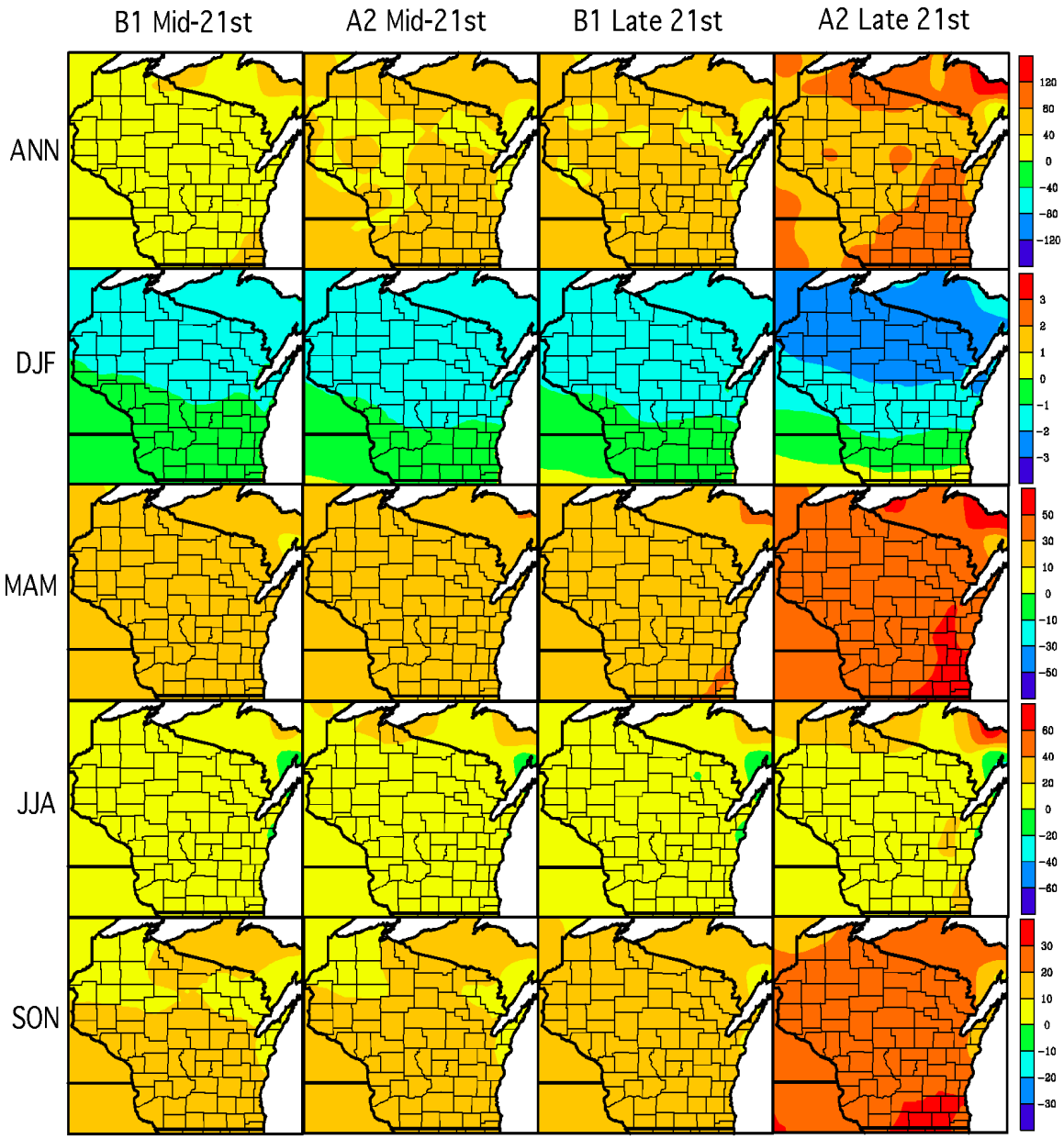

Figure 19. Projected change in Wisconsin's potential evapotranspiration, based on the Priestley-Taylor (1972) method, both annually (mm/year) and seasonally (mm/season) for the mid- and late 21st century and for both A2 and B1 emission scenarios.

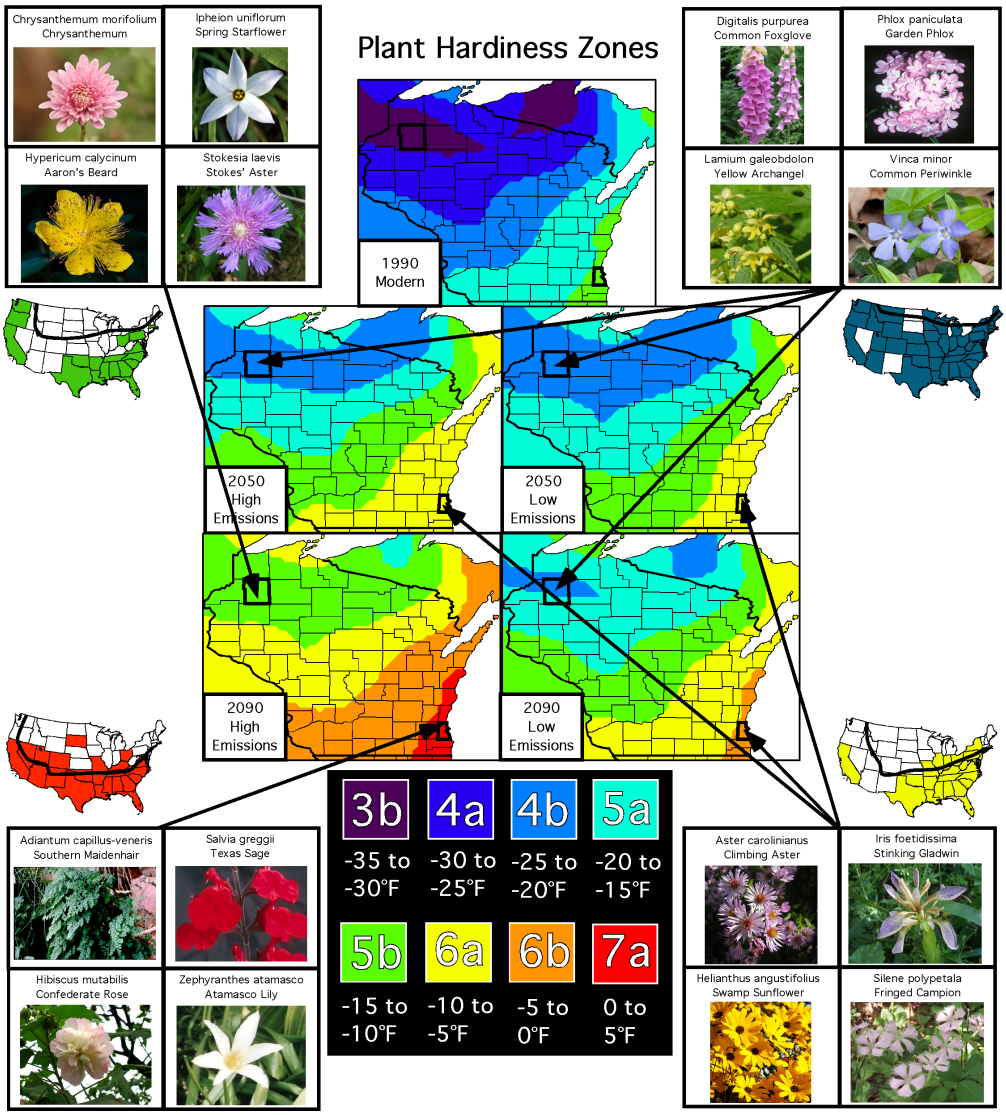

Figure 20. Maps of Wisconsin's plant hardiness zones, for modern-day and projected for years 2050 and 2090, under both high and low greenhouse gas emission scenarios, based on WICCI climate data. Warming will likely change Wisconsin's present-day hardiness zone range of 3b-5b to 4b-6b under a lower emissions scenario or to 5b-7a under a higher emissions scenario by 2090. Sample perennial plant species that might begin to flourish in Wisconsin gardens are shown for Milwaukee and Washburn counties. For example, by 2090, plants such as Texas Sage and Confederate Rose might become a norm in many Milwaukee County gardens. For each set of four plants, a U.S. map is shown with the current USDA-based distribution of all four plants shaded and a line representing the leading edge of the associated hardiness zone for those plants.
Photo sources: Common maidenhair (Gary Larson @ USDA-NRCS PLANTS Database / USDA NRCS), Texas sage (**www.easybloom.com**, crediting photo to **www.centergreenhouse.com**), climbing aster (**www.ncwildflower.org**, crediting photo to Tom Harville, NCBG), swamp sunflower (**www.finegardening.com**, crediting photo to C. Dwayne Jones), fringed campion (**www.fws.gov**), garden phlox (Robert H. Mohlenbrock @ USDA-NRCS PLANTS Database / USDA SCS), and remaining plants (upload.wikimedia.org/wikipedia). Plant hardiness zone ranges for individual plant species are obtained from Armitage (1997).